The effects of small density differences at large confluences

Erik van Rooijen

TU Delft Delft University of Technology

Deltares Enabling Delta Life

NUS National University of Singapore

The effects of small density differences at large confluences

by

Erik van Rooijen

15 November 2016

Graduation Committee:

Prof. dr. ir. W.S.J. (Wim) Uijttewaal	Delft University of Technology (chairman)
Dr. ir. C.J. (Kees) Sloff	Delft University of Technology, Deltares (daily supervisor)
Dr. ir. E. (Erik) Mosselman	Delft University of Technology, Deltares (second reviewer)
Dr. Yuan, J. (Jing)	National University of Singapore (supervisor)
Dr. Chua, V.P. (Vivian)	National University of Singapore (examiner)
Dr. Ooi, S. (Seng Keat)	National University of Singapore (examiner)

Contents

List of figures and tables

List of symbols

A	conveyance area (m^2)
AoO	Amount of overturning (m)
a	acceleration (m/s^2)
c	celerity (m/s)
d	depth of the layer (m)
c_f	Friction coefficient (-)
Fd	Densimetric Froude number, ratio between the propagation of a density current and advection (-)
g	gravitational acceleration (9.81 m/s^2)
h	depth (m)
h_b	Bed height with respect to some horizontal reference height (m)
h_c	current depth (m)
Δh_c	change in current depth (m)
i	water level slope (-)
l	length scale (m)
M_r	Momentum ratio (-)
p	pressure (Pa)
Q	discharge (m^3/s)
Ri	Richardson number, ratio between velocity of a density current and advection (-)
s_w	shear stress due to wind (N/m^2)
s_s	shear stress on the interface between the two layers (N/m^2)
s_b	shear stress due to bed friction (N/m^2)
S	Stability parameter (-)
t	time (s)
T	temperature (°C)
V_s	Fraction of the volume taken up by sediments (-)
u	velocity (m/s)
u_c	velocity in the center of the mixing layer (m/s)
Δu	difference in velocity between the tributaries (m/s)
x	horizontal distance (m)
z	vertical distance (m)
α	entrainment coefficient (-)
δ	Width of mixing layer (m)
κ	von Karman constant (0.4)
ν	Kinematic viscosity (m^2/s)
ρ	density (kg/m^3)
$\Delta\rho$	density difference (kg/m^3)
ρ_s	sediment density (kg/m^3)
σ	sediment concentration (kg/m^3)
ς	salinity (‰)

Preface

The main topic of this report is the effect small density differences can have on the flow downstream of a confluence. This research originally started off as an investigation into the confluence of the Rio Negro and Solimões rivers merging into the Amazon near Manaus, Brazil; one of the largest and most fascinating confluences in the world. Some parts of this initial research can still be found in this report.

However after some time I found that my models produced some unexpected behaviour (dense water moving upwards). I focussed my research on this initially unexpected behaviour, what effects it has, how we can see this in nature and where else we may see it too.

This report is written for anyone who is interested in this subject. However while writing this report I assumed that most people interested would have a background in fluid dynamics. As a result I did not include fundamental or basic theories and formulas from this field since I expected most readers would grasp the essence of this report without needing that information. Throughout the chapters several formulas are used of which the symbols are clarified in the List of symbols.

I would like to thank everyone who has helped me with the research carried out which led to the writing of this report. Most specifically I would like to thank Wim Uijttewaal, Kees Sloff, Erik Mosselman and Jim Best for their help and ideas, which helped shape the research and report to its current state. Also I would like to thank Rob Uittenbogaard for his help concerning the use of the Horizontal Large Eddy Simulation (HLES) module of Delft3D.

Erik van Rooijen
Delft, 15 November 2016

Abstract

Confluences are special, complex elements within river systems which have been subject of much research. However, little attention has been given to the effects of density differences in confluences. The aim of this research is to see when and how density differences are important in confluences with respect to other occurring flow structures. Non-dimensional flow parameters will be linked to certain types of flow. These non-dimensional parameters can then be used to determine to some degree which flow processes can occur.

Using numerical simulations of a schematized confluence the effects of density differences were identified. These effects were visible on several aerial photographs of large confluences. For one specific confluence, the Rio Negro – Solimões confluence near Manaus, Brazil, a separate model was made and run.

The numerical simulations show that the denser water flowed under the lighter water. In a cross-section the shape of the interface between the two waters is very similar to the shape in a lock-exchange. In downstream direction the horizontal part of the interface moves upwards and eventually reaches the surface. This limits the distance over which the two waters can move over one another

If the river downstream of the confluence is insufficiently wide, another process occurs. If the dense or light water reaches the opposite bank, it will well up or down respectively.

When in a confluence a velocity difference is present between the two tributary rivers, a mixing layer is likely to develop. However, density differences can cause motion perpendicular to the main direction of flow. This motion hampers the development of a mixing layer. If density differences become too large compared to the velocity difference, the mixing layer may not develop at all.

We found similarities between the flow characteristics in the numerical models and those visible on aerial photographs of several large confluences. Only aerial photographs with a colour difference between the two tributaries were used.

The numerical model of the Rio Negro – Solimões confluence shows similar characteristics as those in the schematized numerical model. Aerial photographs of this confluence did not show these characteristics. The reason for this is boils of heavier Solimões water at the Rio Negro side of the river disturbed a clear surface pattern. These boils do indicate however that heavy water is present under the lighter water.

Oblique photographs of this confluence often showed the absence of a mixing layer and the presence of floating foam around the interface of the two waters. These two observations can be explained by the theory derived from this research.

This research shows that small density differences can have a significant impact on the hydrodynamics downstream of a confluence. It proved to be possible to link non-dimensional parameters to certain types of flow. However many aspects are still unknown and more research into these is recommended.

1. Introduction

Confluences are fascinating locations in river systems. They are locations where two rivers merge. Especially if these two rivers come from very differing regions, they can have very different characteristics such as velocity, temperature, colour, density and sediment concentration.

The effects density differences can have on the flow downstream of a confluence have not yet been determined in detail. Rare examples of research into the effects of density differences in confluences are the work by Cook & Richmond [2004], Lyubimova et al. [2014] and Best et al. [personal communication]. The density differences can influence the local hydrodynamics and is as such important for sediment transport problems, ecological studies or the routing of a pollutant [Benda et al., 2004; Ardura et al., 2013; Blettler et al., 2014].

However, it is already known that density differences can have significant influences on the flow in for instance estuaries [Vreugdenhil, 1970]. In estuaries the main cause for a density difference is a salinity difference, in confluences a density difference will more likely be caused by a temperature or sediment concentration difference. Such temperature or sediment concentration differences can in turn be caused by differences in albedo, differences in land use or climate zone the tributaries come from or a discharge from a power plant not far upstream of one of the tributaries.

The main aim of this research is to see how and when density differences are important in confluences with respect to other occurring flow structures. Non-dimensional flow parameters will be linked to certain types of flow. These non-dimensional parameters can then be used to determine to some degree which flow processes can occur.

The main question of this research is: “can we give a good approximation of the flow mechanisms which will occur in a confluence with dissimilar densities, based on easily measurable non-dimensional parameters?”

We considered a schematized confluence with a confluence angle of 0°. The flow in this schematized confluence was numerically computed for various flow cases. The results from these flow cases were compared to each other and interpreted. The results from the model were compared to aerial photographs of large confluences and similarities between the two were found. Finally a case study of the Rio Negro – Solimões confluence was undertaken to determine if the same effects also occurred in this confluence.

This research shows the importance that small density differences can have on the local hydrodynamics near a confluence. The processes are explained and a diagram is presented with which the processes occurring at a confluence can be predicted.

2. Theory and literature

2.1 Main characteristics of confluences

Complex flows can occur near a confluence. These flows will have an effect on the mixing of the waters of these two tributaries downstream of the confluence.

Best [1987] made a model for the flow dynamics that often occur at a confluence, see Figure 1. A **stagnation zone** occurs right after the confluence apex. Downstream of this stagnation zone a **shear layer** between the two tributary flows is located. In this shear layer a large portion of the mixing takes place. The location of the shear layer is dependent on the momentum ratio between the two tributaries (1 and 2), defined as: $M_r = \frac{u_1 Q_1 \rho_1}{u_2 Q_2 \rho_2}$ [Best & Reid, 1984]. A momentum ratio close to 1 signals a situation in which the shear layer is located approximately in the middle of the channel.

A **flow separation zone** can develop next to the banks of the main stream right after a tributary flows into the main stream. Often one or both of the waters of the tributaries are deflected a little downstream of the stagnation zone leading to a smaller conveyance area. The deflection can be enhanced by the separation zone leading to an even smaller width for the water to flow through [Best & Reid, 1984]. **Maximum velocity** often occurs where the flow is at its narrowest. These different zones of flow have also been seen in the field, for instance by Rhoads and Sukhodolov [2001].

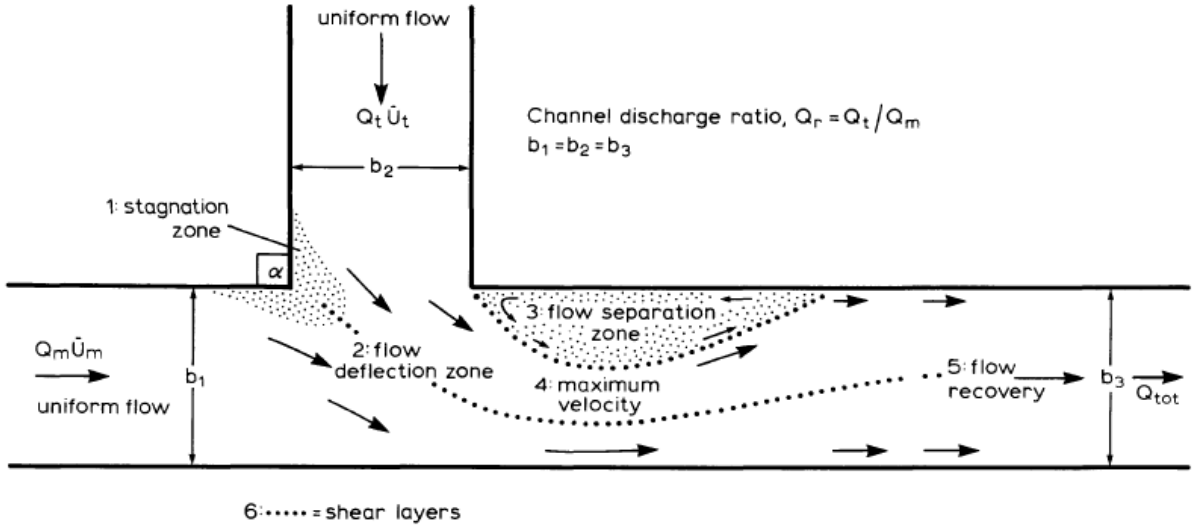

Figure 1 Overview of the flow at a confluence, after Best [1987]

2.2 Confluences and meanders

Often a comparison is made between meanders and confluences. The incoming channels will need to realign themselves to the main channel. The water from the tributaries thus has a curved pathway, which can cause a helical flow pattern as seen in meanders [Ashmore & Parker, 1983; McLelland et al., 1996; Bradbrook et al., 2000a; Rhoads & Sukhodolov, 2001; Huang et al., 2002, Miyawaki et al., 2010]. This analogy works better for more symmetrical confluences (confluences with similar curvature of the tributaries), Bradbrook et al. [2000a] found. When one of the tributaries is much stronger (in terms of momentum) than the other, only one large helical cell will form [Rhoads & Kenworthy, 1995].

A scour hole can develop in the middle of the channel just downstream of the confluence apex as both tributaries will have a deflection of the near bed velocity (and sediment laden water) caused by the curvature induced flow [Best, 1987]. This is similar to a meander where erosion occurs at the outer bank. However a scour hole can also develop more downstream in the area with maximum velocities (the narrowest part) [Rhoads & Kenworthy, 1995].

2.3 Discordant beds

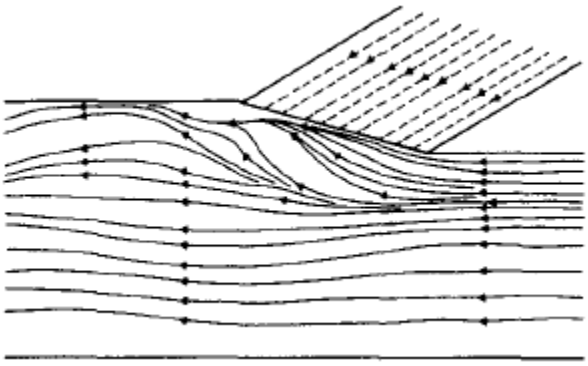

Figure 2 Plan view of stream lines at the bed for a confluence with discordant beds, after Biron et al. [1996]

In a river mixing of a tracer or pollutant is considered a slow process and it can take up to 100-300 times the width of the river in downstream direction to be fully mixed [Biron et al., 2004]. At the mouth of a tributary an avalanche face can develop due to flow deflection, acceleration and increased shear stresses [Best, 1987; Biron et al., 1993]. If such avalanche faces develop this inherently means that the bed levels of the tributaries are not equal to those of the main stream. Biron et al. [1993; 2004] have shown that mixing can happen a lot faster than 100-300 times the river width in confluences with discordant beds; up to 55 river widths. The process taking place in a confluence with discordant beds (unequal tributary bed level) is that water from the tributary with the lower bed level will flow under the water of the tributary with the higher bed level [Biron et al., 1993; 1996; 2004; De Serres et al., 1998], see figure 2. This phenomenon may lead to upwelling of water from the tributary with the lower bed at the bank of the tributary with the higher bed, somewhat downstream of the confluence. This phenomenon will often destroy helical flow cells [Biron et al., 1996].

2.4 Mixing & shear layer

Location of the shear layer

At a confluence a large part of the mixing takes place around the shear layer. There a mixing layer will develop which starts at the confluence apex and generally widens in downstream direction [Winant & Browand, 1974; Uijttewaal & Booij, 2000; van Prooijen & Uijttewaal, 2002]. The mixing layer is a certain length over which a velocity gradient is acting. Just after the two streams meet, the shear layer is vertical. More downstream this is not necessarily the case.

Due to the process following from bed discordance described earlier the shear layer can be shifted laterally along the bed [Biron et al., 1996, De Serres et al., 1998]. The mixing interface generally shifts towards the side of the slower moving fluid [Kirkil, 2015].

Width of the mixing layer

The width of the mixing layer depends for a large part on the velocity difference on the two sides of the mixing layer and the depth of the flow [van Prooijen & Uijttewaal, 2002]. Winant & Browand [1974] note that the maximum width of mixing layer will be in the order of the depth. The width of the mixing layer can increase due to discordant beds [Biron et al., 1996]. At higher Reynolds numbers the mixing layer stops developing earlier [Kirkil, 2015].

Van Prooijen & Uijttewaal [2002] found that the width of the mixing layer, defined as the velocity difference divided by the velocity gradient in the middle of the mixing layer, can be calculated using:

$$\delta(x) = \alpha \frac{\Delta u_0}{u_C} \frac{h}{C_f} \left(1 - e^{-\frac{C_f}{h}x}\right) + \delta_0 \quad (2.1)$$

Where C_f can be computed using:

$$\frac{1}{\sqrt{\frac{1}{2}C_f}} = \frac{1}{\kappa}\left(\ln\left(\frac{uh}{\nu}\sqrt{\frac{1}{2}C_f}\right) + 1\right) \quad (2.2)$$

α had a value of 0.085. We can see from this formula that the maximum mixing layer width is solely dependent on the velocity difference to mean velocity ratio and the depth to roughness ratio (δ_0

tends to be small, in the order of the width of the upstream bank boundary layer, which is in the order of the depth). The mixing layer growth is larger if it is further away from its maximum width.

Mixing layer types

Daoyi & Jirka [1998] showed that there is a stability parameter S for mixing layers which provides a condition for which mixing layers can become unstable. An unstable mixing layer can display large coherent structures like the well-known Kelvin Helmholz instability. If the stability parameter $S = \frac{2c_f l\overline{u}}{h\Delta u}$ has a value higher than 0.0945 to 0.101 the flow is stable and no large coherent structures can develop.

In natural confluences the 'mixing layer' can have different types of large coherent structures. It can behave like a wake just downstream of the confluence apex or more like a classical mixing layer further downstream [Rhoads & Sukhodolov, 2008]. Miyawaki et al. [2010] found in the confluence of the Kaskaskia and Copper Slough that depending on the discharges of the tributaries the 'mixing layer' can behave in two ways: (1) wake-like, with alternating clockwise and counter clockwise rotating eddies being shedded from the confluence apex and (2) mixing layer like, where typical Kelvin-Helmholtz instabilities appear. It appears that the main reason for the difference between these two characters is the location where the flow detaches from the wall. The closer the detaching happens to the confluence apex the more likely the pure mixing layer character will be. It is expected that the geometry of the confluence apex has the largest influence on which type will occur. Constantinescu et al. [2011] found that a situation with a momentum ratio closer to 1 favours the wake-like eddies formation. Herrero et al. [2016] found wake-like eddies being shedded behind the confluence apex in a laboratory study.

Turbulence in mixing layers

In most laboratory experiments Kelvin-Helmholtz instabilities formed just after the start of the mixing layer [Winant & Browand, 1974; Biron et al., 1996; McLelland et al., 1996; van Prooijen & Uijttewaal, 2002]. Sometimes they are also evident in the field [Bradbrook et al.; 2000b, Sukhodolov & Rhoads, 2001; Rhoads & Sukhodolov, 2004]. If the mixing layer extends long enough these individual Kelvin-Helmholtz instabilities can roll-up and merge, forming irregular vortices [Winant & Browand, 1974]. Within the mixing layer higher levels of turbulence can be found [De Serres et al., 1998; Sukhodolov & Rhoads, 2001; Rhoads & Sukhodolov, 2008] which enhances mixing. The turbulence in the shear layer can be classified as quasi-two-dimensional [Sukhodolov & Rhoads, 2001]. The horizontal scale tends to be much larger than the vertical scale which is most evident in the laboratory. Only the smaller scale turbulent motions can then be classified as fully three dimensional.

2.5 Density differences

When the density changes over a cross-section downstream of a confluence but the water head does not change over the cross section a secondary current will be formed. As a result of these different densities the water levels will differ. Figure 3A shows the water pressures over the vertical for a case with different densities. Note that the triangles are of equal size (so the total force to the right is the same as the total force to the left). At the top of the water columns the lighter water pushes harder whereas at the bottom of the water column the heavier water pushes harder. This causes the heavier water to flow under the lighter water and the lighter water to flow over the heavier water. Similar figures can be made for a density difference over only a part of the water depth (Figure 3C), which occurs for instance at the head of a density current.

The acceleration of the water is proportional to the pressure gradient: $a = \frac{du}{dt} \sim \frac{dp}{dx}$. From Figure 3A we can see that: $\frac{d}{dz}\left(\frac{dp}{dx}\right) = C_1$ and hence: $\frac{d}{dz}\left(\frac{du}{dt}\right) = C_2$, assuming no bottom friction. When the head of the density current has passed (and the lighter water is on top of the heavier water with a horizontal separation) $\frac{dp}{dx}$ will be 0 (Figure 3B). No acceleration will occur, and if we

assume no friction, the velocity will be constant. Only acceleration will occur at the head of the density current (Figure 3C).

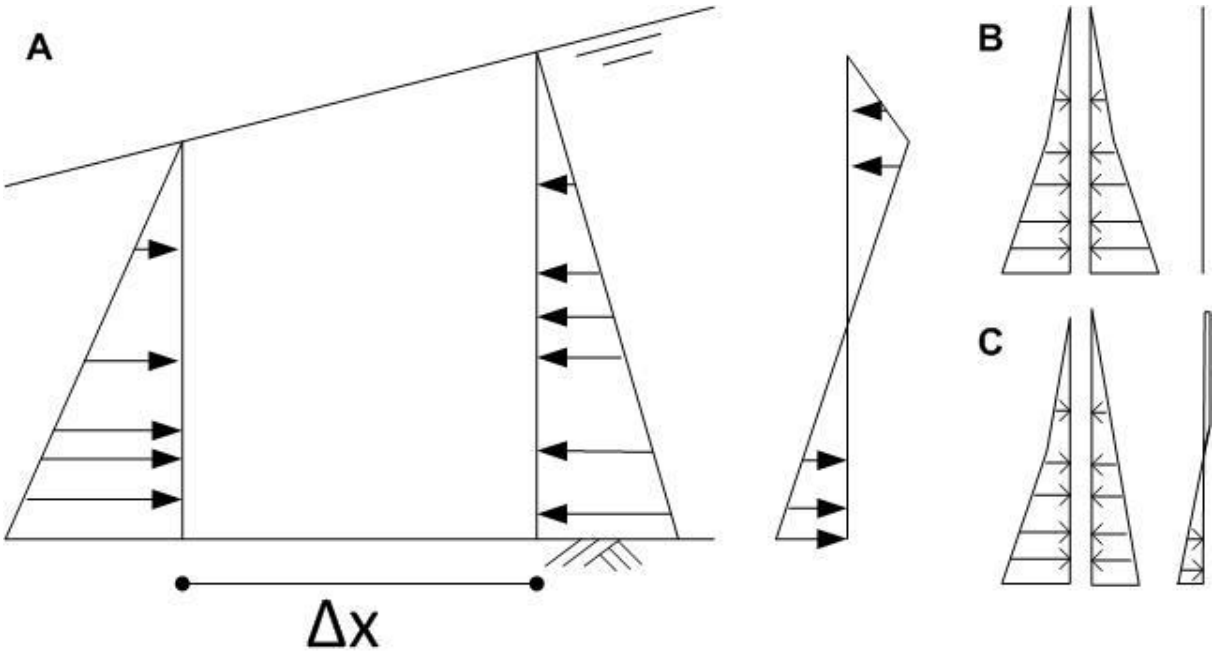

Figure 3 Water pressures on a small partition of water with width Δx under influence of density differences and resulting pressures. A. Differing densities over the entire water column. On the right side is the low density water and on the left side the high density fluid. Water level differences are exaggerated. As a result in reality the small part at the top of the resulting pressures profile where the pressure is linearly increasing with depth will be so small it can be neglected. B. Stratified situation. C. Head of a density current.

One of the most classical problems concerning density currents is that of the lock exchange. Two bodies of water with different densities are placed in a flume and are separated by a vertical separation. At the start of the experiment this vertical separation is quickly removed and the heavier fluid will flow over the bottom towards the lighter fluid and the lighter fluid will flow in the opposite direction near the surface [Benjamin, 1968; Kneller et al., 1999; Shin et al., 2004].

Figure 4 A lock release with heavy (dark) and light (light) water. The dashed line indicates Benjamin's [1968] potential flow solution for the shape at the fronts, joined by a horizontal line. After Shin et al. [2004].

The speed of the two fluids moving towards the other fluid is constant in time [Benjamin, 1968; Kneller et al., 1999]. Benjamin [1968] derived this celerity from the Bernoulli equation:

$$c = \frac{1}{2}\sqrt{g\frac{\Delta\rho}{\rho_2}h_c} \quad (2.3)$$

In the derivation of this formula the effect of the viscosity and (bed) friction is ignored.

The situation at a certain point in time could be schematized as two parts with a potential flow solution as described by Benjamin [1968] which are joined by a horizontal line [Shin et al., 2004], see Figure 4. The shape and orientation of the vertical separation which is to be removed seemed to have an impact on the flow [Shin et al., 2004]. The horizontal interface is located at approximately half the depth in the case of small density differences [Benjamin, 1968].

2.6 The two-layer model

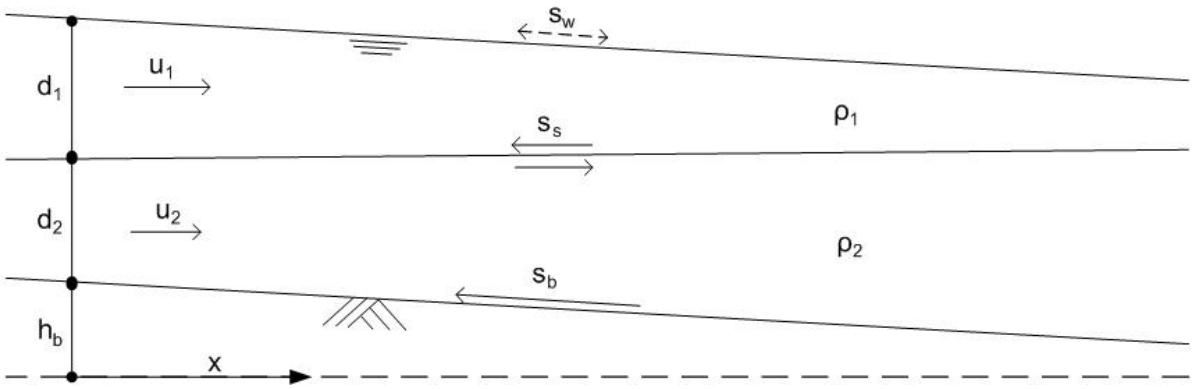

Figure 5 Overview of the used parameters in the two-layer model.

If a flow is vertically stratified we can derive two equations for the heavy water and two equations for the light water based on conservation of mass and momentum. This method is called the two-layer model [Schijf & Schönfeld, 1953]. Kranenburg [1998] shows that the equations for mass balance and momentum balance in the case of two layers are:

$$\frac{\partial d_1}{\partial t} + \frac{\partial}{\partial x}(d_1 u_1) = 0 \quad (2.4)$$

$$\frac{\partial d_2}{\partial t} + \frac{\partial}{\partial x}(d_2 u_2) = 0 \quad (2.5)$$

$$\frac{\partial u_1}{\partial t} + u_1 \frac{\partial u_1}{\partial x} + g \frac{\partial}{\partial x}(h_b + d_1 + d_2) = \frac{s_w + s_s}{\rho_1 d_1} \quad (2.6)$$

$$\frac{\partial u_2}{\partial t} + u_2 \frac{\partial u_2}{\partial x} + \frac{\rho_1}{\rho_2} g \frac{\partial d_1}{\partial x} + g \frac{\partial}{\partial x}(h_b + d_2) = \frac{s_s + s_b}{\rho_2 d_2} \quad (2.7)$$

In these equations the subscripts 1 and 2 refer to the top layer and bottom layer respectively. In Figure 5 the different parameters used in the equations are shown visually. Note that in equations 2.6 and 2.7 the magnitude of s_s is the same but in 2.6 s_s is negative and in 2.7 it is positive (due to Newtons third law).

The two-layer model assumes that little mixing is taking place along the interface between the two layers. It also assumes that both layers have the same velocity throughout the entire layer. The shear stress between the two layers s_s is dependent on the velocity difference between the two layers.

2.7 Density differences in confluences

Based on experiments using different gasses Brown & Roshko [1974] concluded that density differences generally have little influence on the mixing layer. They found that an increase in density ratio with a factor 49(!) keeping the velocity ratio constant causes a decrease in spreading angle of roughly a factor 2. Note that these experiments were done with much higher density differences than ever possible in normal river flow.

Density differences can have an influence on the flow structure at a confluence however. At the Clearwater and Snake rivers Cook & Richmond [2004] found that water from a relatively warm tributary flowed over water from a nearly 10°C-lower-temperature tributary immediately after the confluence. At lower temperature differences this was not seen. Exact density differences were not given, nor flow patterns at intermediate temperature differences.

Lyubimova et al. [2014] found that in a confluence with very low velocities (order 0.05 m/s) and with density differences, water from one tributary could end up upstream of the other tributary. I.e. low-density water from one of the tributaries could be found near the surface upstream of the other tributary.

Based on the theory described above we would expect that at a confluence with two tributaries of different densities, the heavier water will flow under the lighter water. The profile that

would develop should be similar to the one of a lock exchange. It is expected that in downstream direction the width over which one of the waters is on top of the other is increasing. In other words, we expect a stationary flow, in which a lock exchange process is occurring in space instead of in time. In the lock exchange usually the overturning, the distance over which one of the waters has moved over the other, increases in time. Here the overturning increases in space because it is advected by the mean flow. It is therefore expected that when the mean flow increases the overturning occurring over the same distance would decrease. It is also expected, see Eq. 2.3, that the depth and density difference have an influence on the rate of overturning. When water from one of the tributaries gets to the bank of the other tributary up- or downwelling is expected, similar to what Biron et al. [1996] saw.

Boyer et al. [2006] described the effect of the shear layer on the morphology. Because of this we also expect an indirect effect of the density differences on the morphology. This is however outside the scope of this research.

2.8 Boils

A phenomenon we can see in natural rivers are boils or kolks. They can be seen on the surface as areas where turbulent upwelling takes place. They can transport large quantities of water from the bottom of the stream towards the top of the stream, increasing mixing significantly. Sometimes these boils can be seen very well due to the differences in water characteristics (for instance sediment concentration) of the water upwelling and the water in which it upwells. One example of this is just downstream of the confluence of the Bermejo and Paraguay rivers [Blettler et al., 2014].

According to Nezu & Nakagawa [1993] there are 3 different mechanisms that can cause turbulent boils. The first type of boil is most common and occurs downstream of large bedforms, most specifically dunes and large scale ripples [Nezu & Nakagawa, 1993]. Their location is dependent on the location of the bedforms and changes with the change of location of the bedforms. Often multiple boils can be seen close together. They occur both in spanwise direction (due to the same bedform) or streamwise direction (due to multiple bedforms located after each other). Jackson [1976] found that these boils have their origin in the turbulent boundary layer and are often initiated in the trough of bed forms. He also found that the boils increase in size if the bed roughness or the depth of the stream increases.

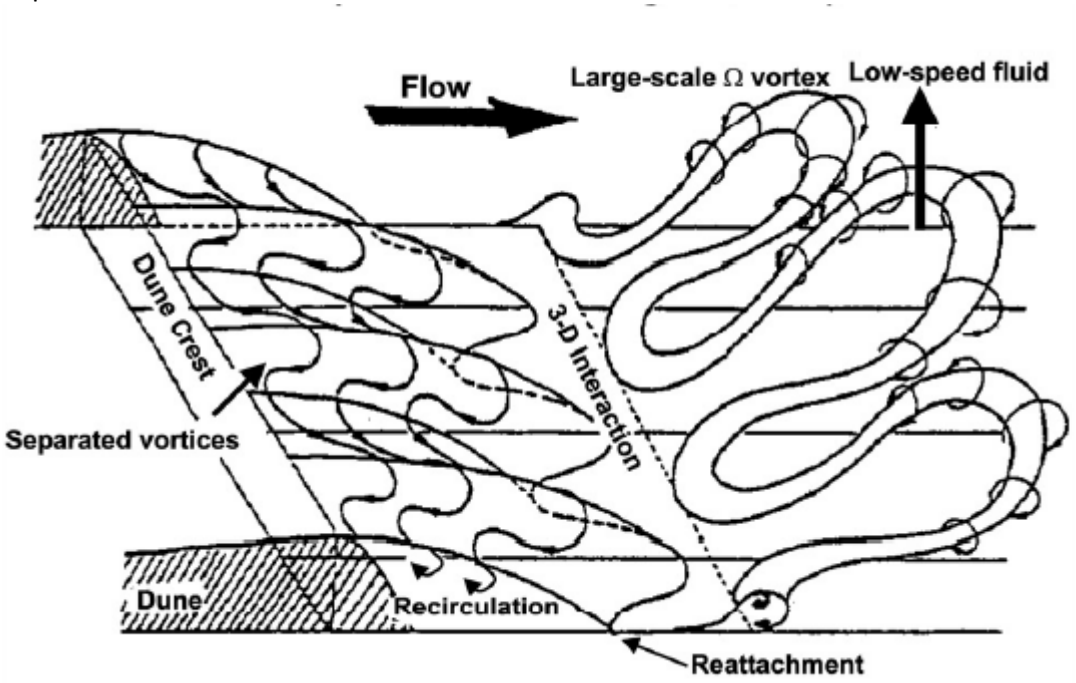

Figure 6 Hairpin vortices downstream of a dune, from Best [2005], originally from Nezu & Nakagawa

According to Nezu & Nakagawa [1993] these boils are caused by the fluctuation of the location of the reattachment point, the location where the flow reattaches with the bed. A high-velocity vortex is shedded from the dune (similar to a mixing layer) coming near to the reattachment point, see Figure 6. Due to entrainment of surrounding water low-frequency motions are introduced at the reattachment point. This results in a hairpin shaped vortex that is shedded from the reattachment point. Experiments show that kolk-boils primarily form during periods of increasing water discharge, after the dunes were fully developed the kolk boils could not be seen anymore [Nezu & Nakagawa, 1993].

Coleman [1969] found such boils on aerial photographs in the Brahmaputra River in what is now Bangladesh. Best [2005] has found such boils in a flume experiment and in the Jamuna (Brahmaputra) river in Bangladesh. He also describes how these boils develop on the surface (so you can recognise them in the field). Similarly to Nezu & Nakagawa [1993], Best [2005] proposes that boils are created by flapping of the shear layer at the lee side of the dunes due to already present turbulent structures from upstream. This causes strong temporary upwelling at the lee side of the dune which in turn causes slower downwelling at other locations and periods (due to mass balance). A horseshoe or hairpin shaped vortex is the result. This vortex is inclined and causes the boil when it reaches the surface, see Figure 6. This is in line with Large Eddy Simulations (LES) of flow over dunes done for low Reynolds numbers [Grigoriadis et al., 2009; Omidyeganeh & Piomelli, 2011]. Zedler & Street [2001] also found such hairpin shaped vortices behind small ripples in their LES, these however never reached the water surface.

The second way boils can surface is due to a process very similar to secondary currents [see Nezu & Nakagawa, 1993; Nezu et al., 1993; Albayrak, 2008]. The main difference is that in this case the process is not constantly occurring but only temporarily. This type of boils are usually located in streamwise lines located approximately equally far away from each other [Nezu & Nakagawa, 1993].

The last mechanism causing boils is by burst events. Close to the bed areas with relatively high speed and low speed collide; at the colliding interface a vortex develops with a hairpin or horseshoe shape which is inclined and moves upwards. This vortex may reach the surface where it will then cause a boil which is described as very weak and hard to notice. It occurs primarily on flat bottomed streams. It should appear completely random in both time and space [Nezu & Nakagawa, 1993].

Albayrak [2008] found that possibly the third type of boil can interact with secondary currents. The secondary currents can suppress the boils from coming to the surface at locations of downwelling whereas they stimulate getting boils to the surface in areas of upwelling.

3. Methods

3.1 Numerical modelling

Investigating the effects of small density differences on the hydrodynamics downstream of a confluence is difficult to do in nature. This is especially the case if the confluence is large. Measuring is a very time and resource intensive task and many measurements of different confluences at different flow regimes would be necessary.

Numerical modelling generally doesn't have these drawbacks. An additional advantage of numerical modelling is that hypothetical cases can be studied. This is in particular a handy feature when investigating the effect of a single parameter, because numerical modelling allows us to change only this one parameter. This is impossible in nature. In this study the Delft3D [Deltares, 2014] software was used.

Numerical models have many different parameters and modes which can be used. It is of importance to first identify which modes are needed for the specific problem and which are not needed.

3.2 Validation of the software used

Two checks are required to verify that Delft3D can solve the processes of interest well. First a check is needed to verify that Delft3D can properly simulate the development of the mixing layer downstream of a confluence apex which influences the density gradient. The second check is needed to verify that Delft3D calculates density currents well. For the model runs used see also Appendix A.1.

Mixing layer validation

For the first check a numerical model was used. It was to check the proper development of the mixing layer, which influences the density gradient, forming downstream of a confluence apex. The geometry of this model was similar to that of a splitter plate experiment. The grid was 500x81 grid cells of 30 m x 30 m. It had a bed level of -35 m and 20 σ-layers were used. At the upstream boundary the two tributaries were initially separated by several dry points. For each time step the upstream boundary conditions (discharges) were randomly drawn from a Gaussian distribution with a standard deviation of 2%. To allow Kelvin-Helmholtz instabilities to develop the Horizontal Large Eddy Simulation (HLES) was enabled with a relaxation time of 40 minutes. A mean velocity of 1.19 m/s and a velocity ratio between the two tributaries of 3/7 were chosen as they are representative of many large confluences. A rather large velocity ratio was chosen to ensure the development of a mixing layer. The width of the mixing layer found was checked against the theoretical width of a mixing layer (Eq. 2.1) for this case. A numerical tracer was added to one of the tributaries to allow for post-processing.

Density currents validation

The other important aspect is density currents. Delft3D should also be able to solve these properly. Gerritsen et al. [2008] showed that Delft3D needs to run in non-hydrostatic mode to be able to solve the lock exchange (and the density currents) properly. Commandeur [2015] showed that in practical cases the differences between using and not using non-hydrostatic mode are small. A standard model was run with non-hydrostatic mode enabled and disabled, and the results were compared.

3.3 Model runs used

A schematized numerical model of a confluence was used to identify the effects density differences have on the flow downstream of the confluence apex. An overview of the model runs used is given in appendix A.2.

All models were run with a geometry similar to the geometry used in the previous chapter: a rectangular grid with several dry points located in the middle of the upstream boundary separating the two tributaries. The bed level was constant throughout the domain. In such a geometry, bed

discordance or curvature induced flow can have no influence. The base version of the model uses no velocity difference between the tributaries and the density difference is completely caused by a temperature difference to ensure no vertically differing density difference can develop (no Rouse profile can develop).

To identify the effects of the density differences on the mixing layer, the velocity ratio was systematically changed. Also a run with the maximum velocity ratio and only half the density (temperature) difference was executed.

All other models were used to identify how the density currents behaved. The effects of the width, velocity, roughness, depth and temperature difference were investigated by changing these parameters systematically, see appendix A.2. The effect of these parameters on the amount of overturning (AoO) was specifically investigated, see Figure 7. The amount of overturning for a certain cross-section is here defined as the horizontal distance between the locations at the surface and bottom of the water where the density is exactly the unweighted mean density of the two tributaries. In numerical models the space is discretized and as a result rarely the location with the mean density will fall exactly on one grid point. This location was computed by linear interpolation of the neighbouring grid points.

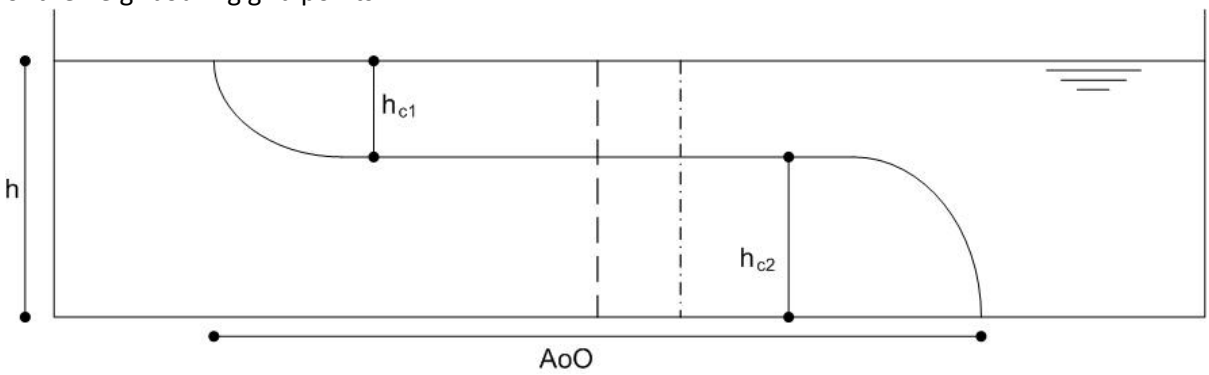

Figure 7 Definitions of several of the used parameters. Shown is a cross-section downstream of the confluence with heavy water right and light water left. The dashed line is the mean location and the dash-point line is the depth averaged location of the shear layer.

Additionally the effect the turbulence closure model had was investigated by also executing one run with each of the other available turbulence models (constant, k-L and algebraic).

The location where the largest overturning occurred was also compared between the model runs. Finally also the mean location of the shear layer was investigated as it gives, together with the amount of overturning, a good idea where water from each tributary ends up. The mean location is then defined as: the mean location between the points at the surface and bottom where the water density is the mean density of the two tributaries. Note that this is not the same as the depth averaged location, see Figure 7.

The different flow characteristics are linked to dimensionless parameters based on the dependencies found. This will be done for the speed at which the two waters flow over each other and the existence of a mixing layer.

3.4 Aerial photographs

Even though numerical models have many advantages they also have their drawbacks. If something happens in a model, it does not mean it will also happen in reality. Therefore a verification needs to take place. In most cases this is done with measurements.

Measuring in a flume of similar dimensions as the one used for the model is impossible due to its large length scales. A smaller flume could be used instead where flow properties are scaled with the Froude number. This will however mean that other flow properties, for instance turbulence properties described by the Reynolds number, would change (unless a fluid with another viscosity is used). These measurements are rather time consuming and therefore did not fit in the available timeframe of this study.

As noted before doing measurements in the field is very time and resource consuming. For validation of course less measurements are required, however due to the nature of large confluences still a lot of effort is needed. Also few measurements are available as is.

Confluences are however special locations in the river. At these locations two rivers, generally with different characteristics, merge. It is not uncommon that a distinguishing characteristic is the colour of the water. Aerial photographs or satellite imagery displaying this colour difference then also yield a very detailed view of the flow field at the water surface. The colour is thus used as a tracer.

These aerial photographs or satellite images were used as verification. Photographs with obstructing clouds could of course not be used. Also the images were only useable if a clear colour difference was present between the two tributaries.

3.5 The confluence of the Rio Negro and Solimões rivers

One confluence site is known for having a small density difference between the two tributaries: the confluence of the Rio Negro and the Solimões merging into the Amazon near Manaus in Brazil, see Figure 8. Luckily some aerial photographs were available for this confluence area too.

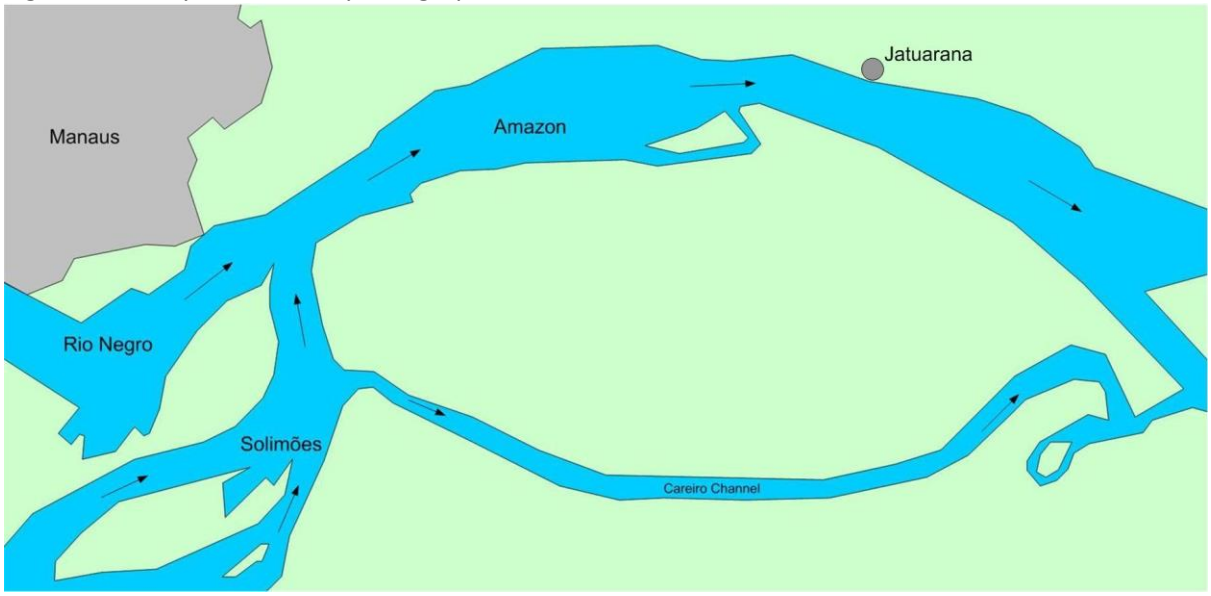

Figure 8 Schematic map of the confluence area of the Rio Negro and Solimões rivers. The arrows indicate the flow direction. The city of Manaus is located in the top left corner of the figure.

The confluence of the Rio Negro and the Solimões is one of the largest in the world. About 12% of all water drained by rivers to oceans and seas passes this site [Molinier et al., 1993; 1996]. Due to the different colours of the Rio Negro (black) and the Solimões (white) which initially flow next to each other without visibly mixing, it is a large tourist attraction [Laraque et al., 2009].

In this confluence the discharge varies drastically over the year [Filizola et al, 2009 and Figure 9]. As a result of this the momentum ratio varies too. The Solimões always has a significantly larger discharge and velocity than the Rio Negro, causing the momentum ratio to be always above 1.

The Rio Negro transports nearly no sediment. The Solimões does however, and the amount changes over the year [Richey et al., 1986].

Laraque et al. [2009] state that lighter Rio Negro water is located above heavier Solimões water. They also found water from the Solimões upwelling near the Rio Negro bank, similar to the process of fluid from a confluence with a lower bed level upwelling near the opposite bank described by Biron et al. [1996].

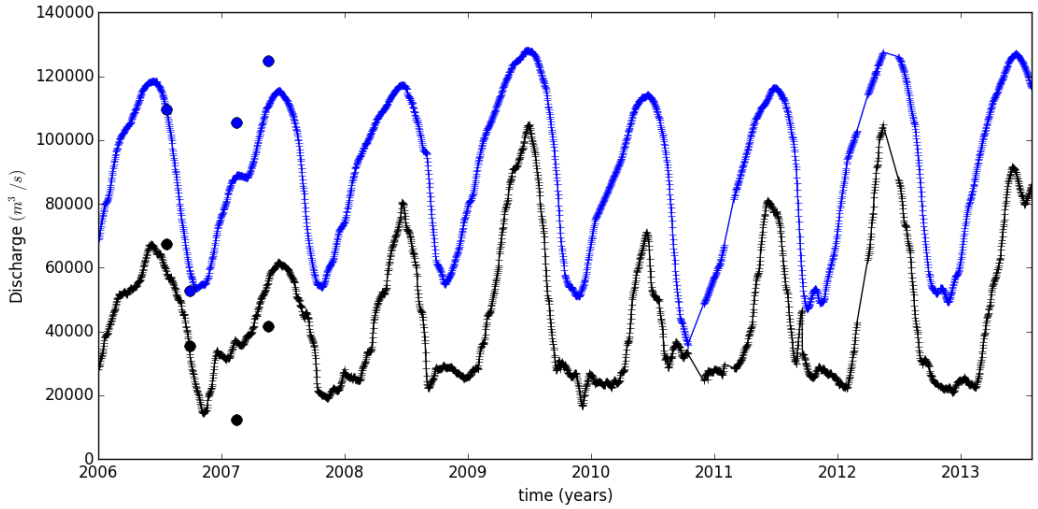

Figure 9 Discharges at the confluence, Solimões (blue) and Rio Negro (black), data from the National Water Agency [ANA 2016], the circles denote measurements from Filizola et al. [2009].

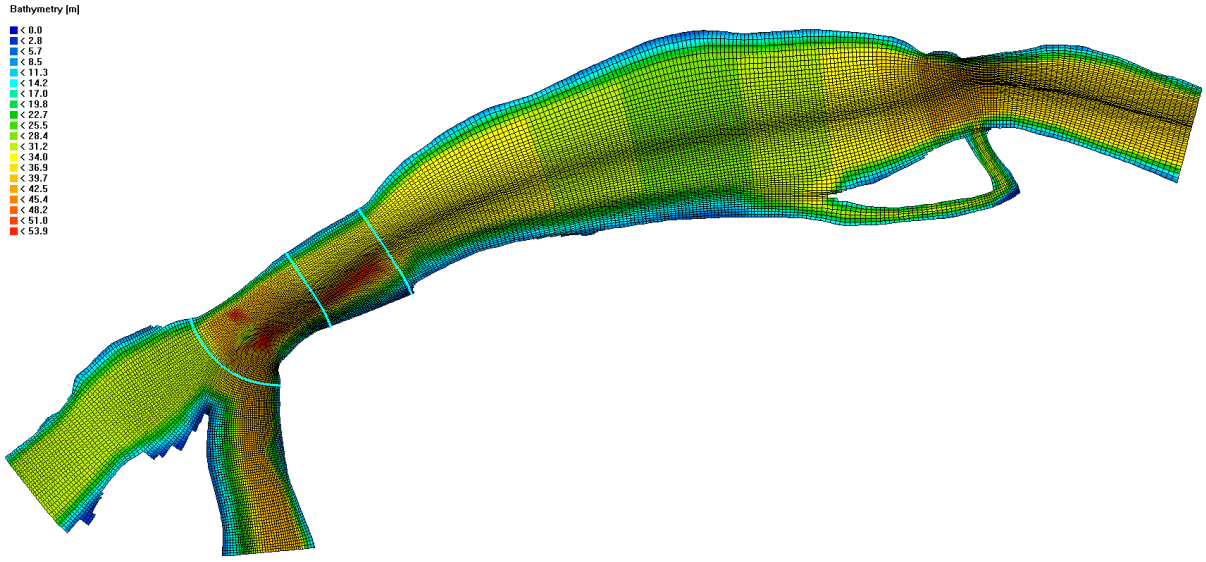

Figure 10 The numerical grid used on top of the bed levels used for the Rio Negro – Solimões model. The three cyan lines are the locations of the cross-sections of Figure 36.

Based on the properties found (measurements) of the confluence a schematized numerical model of this confluence was made; see Table 1 and Figure 10. The upstream (discharge) boundaries were located several kilometres upstream of the confluence apex; on the Solimões River just downstream of the bifurcation with the Careiro channel. So this bifurcation was not part of the numerical model. The downstream boundary was chosen to be at Jatuarana as water level measurements were available there. The sediment concentration had an influence on the density, but no sedimentation or erosion was modelled.

Table 1 Overview of the parameters in the model runs.

	Discharge (m^3/s)[1]		Temperature (°C)		Sediment Concentration (kg/m^3)[4]	
	Rio Negro	Solimões	Rio Negro	Solimões	Rio Negro	Solimões
High Flow	120,000	70,000	31[2]	30.4[2]	0	0.160
Highest Momentum ratio	100,000	30,000	31[2]	30.4[2]	0	0.345
Low Flow	60,000	25,000	31[3]	30.4[3]	0	0.321

1. Based on ANA [2016].
2. Estimated, no data available.
3. Based on Laraque et al. [2009] and Trevethan et al. [2015b].
4. Based on Richey et al. [1986]

It was known that in the Rio Negro – Solimões confluence a significant bed discordance is present [Laraque et al., 2009; Trevethan et al., 2015a]. It is also known that a bed discordance can cause an overturning of the shear layer [Biron et al., 1993; Biron et al., 1996; De Serres et al., 1998]. It would therefore not be remarkable if we would find an overturning of the shear layer due to the bed discordance.

The base version of the model was run with different bed level settings so the effect of the bed discordance could be investigated. Additionally the model was run with z-layers instead of σ-layers, non-hydrostatic calculation, anti-creep correction, different bed level schematizations, smaller grid cells and combinations of these settings to be sure that if the bed discordance had an impact on the overturning it could be found. These runs were done without density differences.

The model was run for three discharge stages: highest momentum ratio, high flow and low flow. These three flow regimes correspond to the months of February/March, July/August and November respectively, see Figure 9 and Table 1. These models could then be compared with the aerial photographs of this site and the more general models used earlier. The model itself was validated against velocity profiles measured by [Trevethan et al., 2015b].

4. Results and discussion

4.1 Validation of the software used

HLES validation

The model used to assess how well Delft3D solves a mixing layer showed clear Kelvin-Helmholtz instabilities, see Figure 11. In Figure 12 the width of the mixing layer is plotted. The blue line represents the width found in the model. The width of the mixing layer was determined as the maximum horizontal distance between two points with a mean tracer amount over a period of 6 hours with a sampling frequency of 5 minutes.

The black line is the theoretical width of the mixing layer described by van Prooijen & Uijttewaal [2002] (equation 2.1) for this case. Note that they define the width of the mixing layer as the velocity difference divided by the velocity gradient in the middle of the mixing layer and that these two definitions are not the same.

The resemblance between the two lines is good however and we can conclude that the Delft3D software gives reasonable results as to the development of a mixing layer. The lines are not on top of each other which is due to the difference in definition. However for our study, in which the density gradient is of largest importance, the correlation is sufficient. The small bumps in the blue line are due to the low sampling frequency. Increasing the sampling frequency could smoothen the line but this was impossible to do due to hardware restrictions.

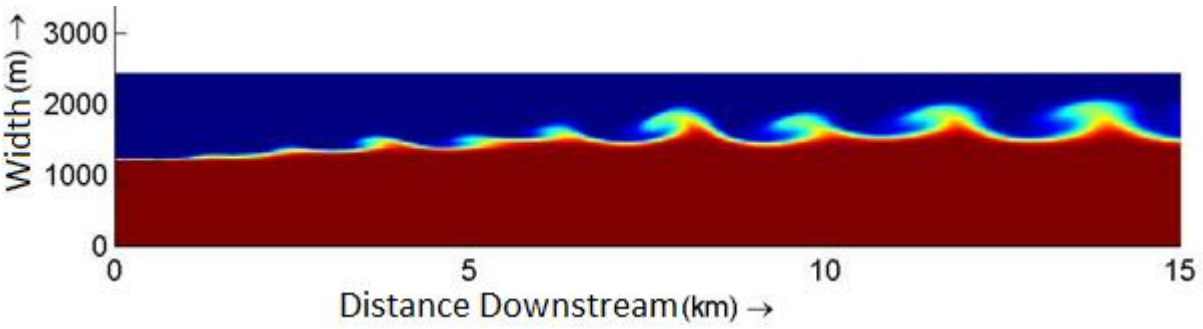

Figure 11 A top view of the model used to assess the characteristics of the mixing layer in Delft3D, showing clear Kelvin-Helmholtz instabilities. The colours indicate the amount of a tracer added to the lower tributary.

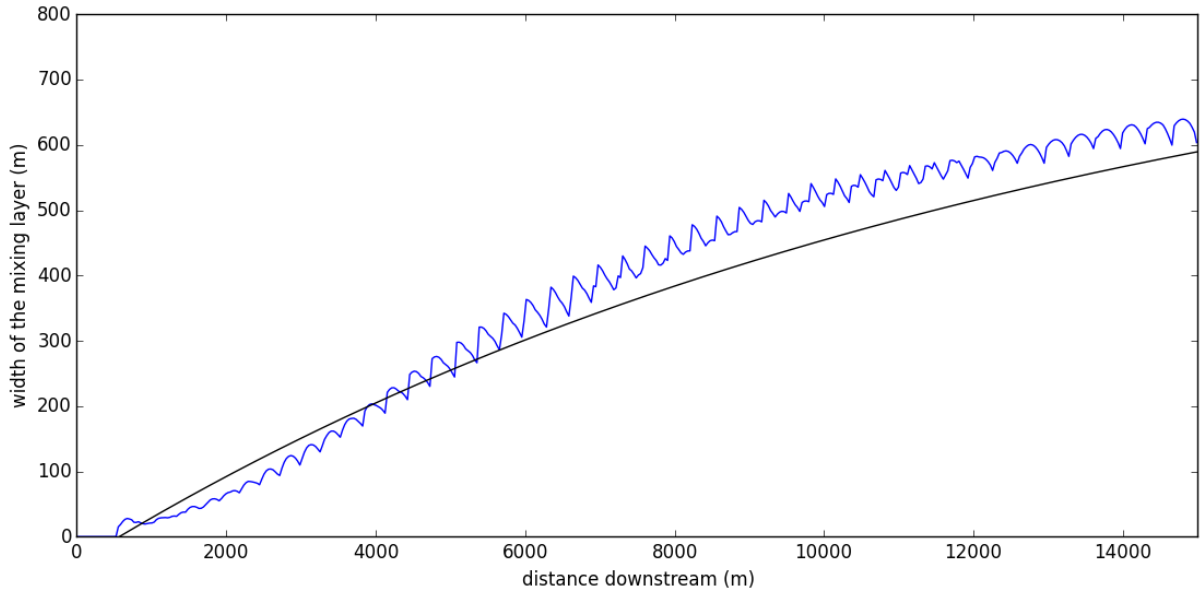

Figure 12 Width of the mixing layer as function of downstream distance. Blue: from model. Black: from theory.

Non-hydrostatic mode required?

Figure 13 shows the densities in an arbitrary cross-section downstream of the confluence apex for computations with σ-layers, z-layers and z-layers with non-hydrostatic mode enabled. The root mean square deviation (RMSD) for the density between the runs using z-layers and non-hydrostatic mode enabled was 0.0003849 kg/m^3. This value is very small compared to the total density difference (about 0.6 kg/m^3) and therefore we can conclude that the non-hydrostatic mode does not have a significant influence. Comparing the results from the runs with σ-layers to those with z-layers it is clear that there are significant differences, the differences were likely caused by the vertical discretization.

Since the bed is flat and the water level is nearly horizontal σ-layers and z-layers should give near identical results. In the z-layer model a little less grid cells were used in the vertical as during the spin-up the water level could become higher. In that case the top layer would not be high enough, to counteract that the elevation of the top of the top grid cell is significantly above the water level. This thus causes that there are less grid cells in the vertical. Because of this also the grid cell interfaces differ a little which could also have a minor influence.

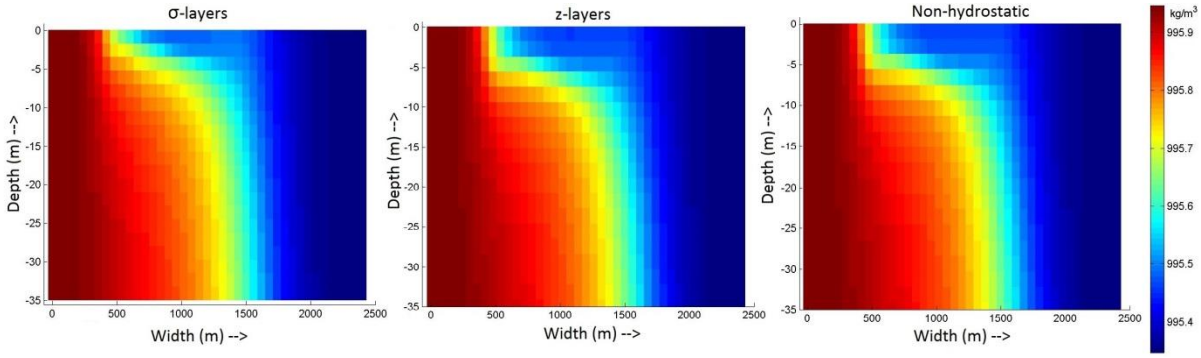

Figure 13 Densities in the same cross section for hydrostatic computation with σ-layers (left), hydrostatic computation with z-layers (middle) and non-hydrostatic computation (right)

4.2 Effects on the large-scale flow pattern

General shape

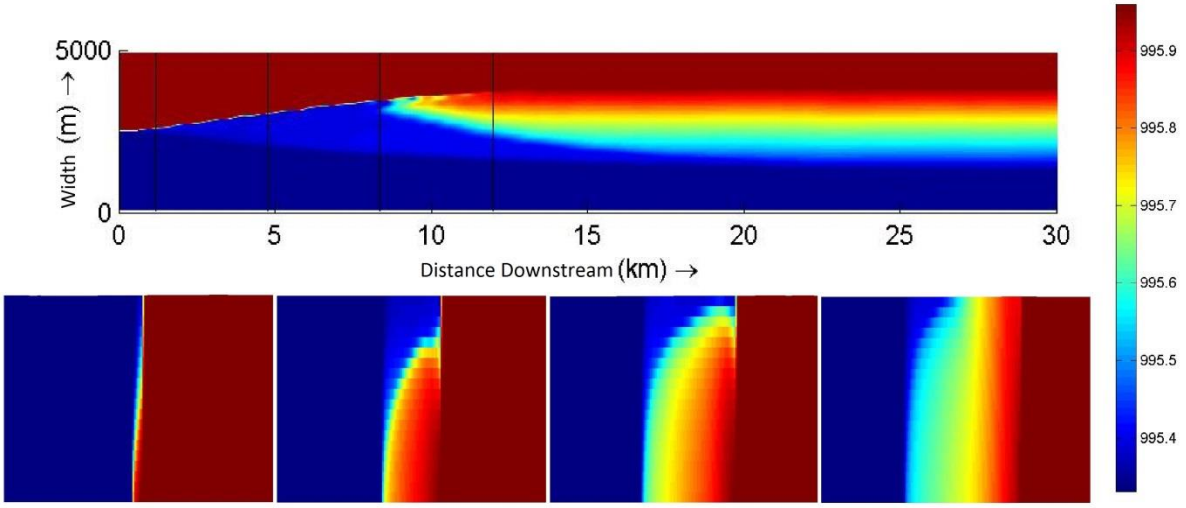

Figure 14 Densities (kg/m^3) in the top layer (flow from left to right) and 4 cross-sections equally far apart (denoted by the black lines in the top figure). The cross-sections give a view to upstream.

Figure 14 shows a top view and several cross sections of the model with the default values (see Appendix B). Note that in this figure the width is 4830 m and the depth is 35 m, the aspect ratio is thus over a 100 and the figures of the cross-sections are distorted. It is clear that the heavier water is flowing underneath the lighter water. A striking feature is however that the horizontal part of the interface is moving upwards. At some point downstream this horizontal interface reaches the

surface and the overturning reduces. Even though a density gradient still exists at this point downstream, no overturning can be seen here. This can also be seen in Figure 15.

It is expected that the density gradient has become so small that the resulting secondary current is very weak and all water transported by this current is quickly mixed with the water already present. This would result in no further overturning from this point onwards.

Water levels (Figure 16) are higher on the low density side. We thus get a situation as shown in Figure 3. The water level slope is the same on the high density as on the low density side.

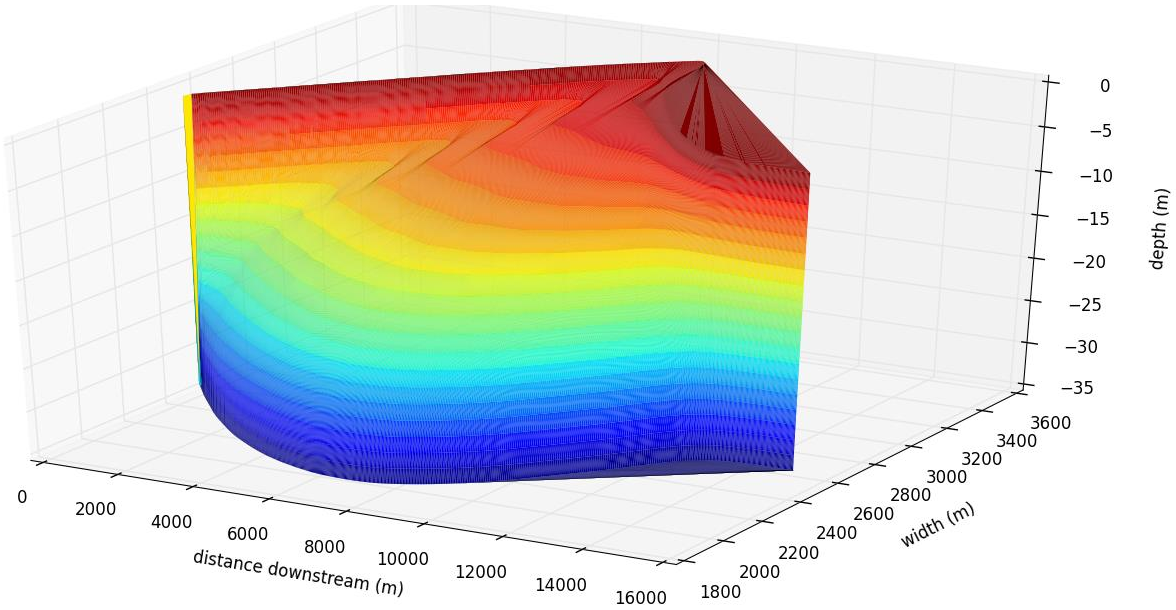

Figure 15 3D image of the time averaged location of the plane with mean densities, colours denote depth.

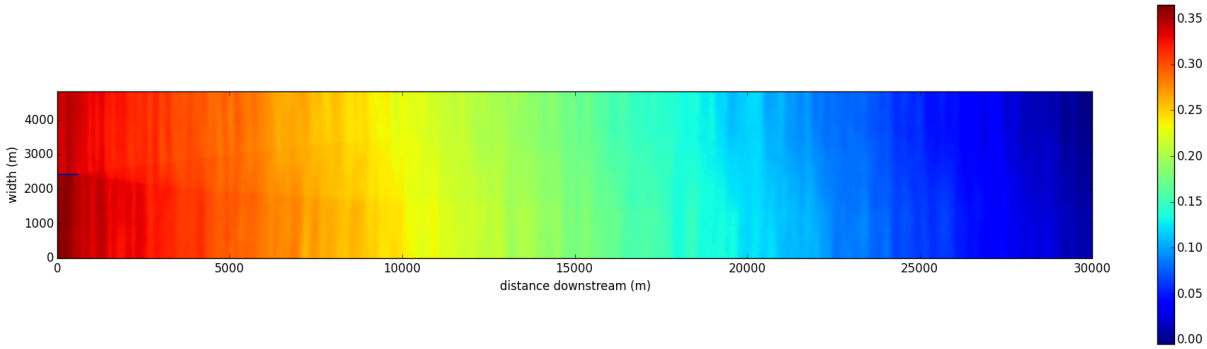

Figure 16 Water levels (m); time-averaged

Figure 17 shows the vertical velocities in a cross-section as well as the velocities in the plane of the cross-section. The density difference causes two density currents (one at the surface of light water and one at the bottom of heavy water). Downwelling is occurring where the interface between the two waters is at the surface and upwelling is located where the interface is at the bottom. The downwelling occurs on the heavy water side and the upwelling on the light water side. The downwelling seems to be stronger than the upwelling. Water in between the areas of up- and down welling generally moves (very slowly) upwards which could explain the difference between the magnitudes of up- and downwelling.

Figure 18 shows the vertical velocities halfway the depth. It is clear that downwelling and upwelling are occurring due to the density differences. The locations where these occur are located further apart from each other in downstream direction. The downwelling is occurring at the location where the shear layer is located at the surface and the upwelling is located where the shear layer is located at the bottom. The streaks perpendicular to the flow of upward and downward moving water are due to the disturbances in the inflow boundary.

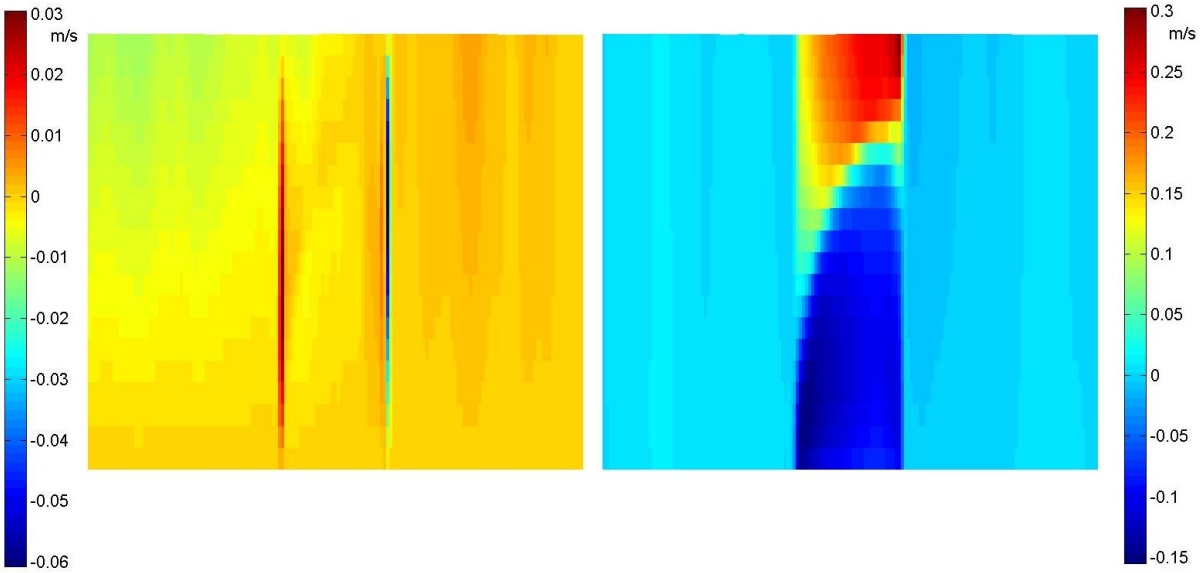

Figure 17 Vertical velocities in a cross-section and velocities in the plane of the cross-section. The cross-section is at the location of the second cross-section of Figure 14.

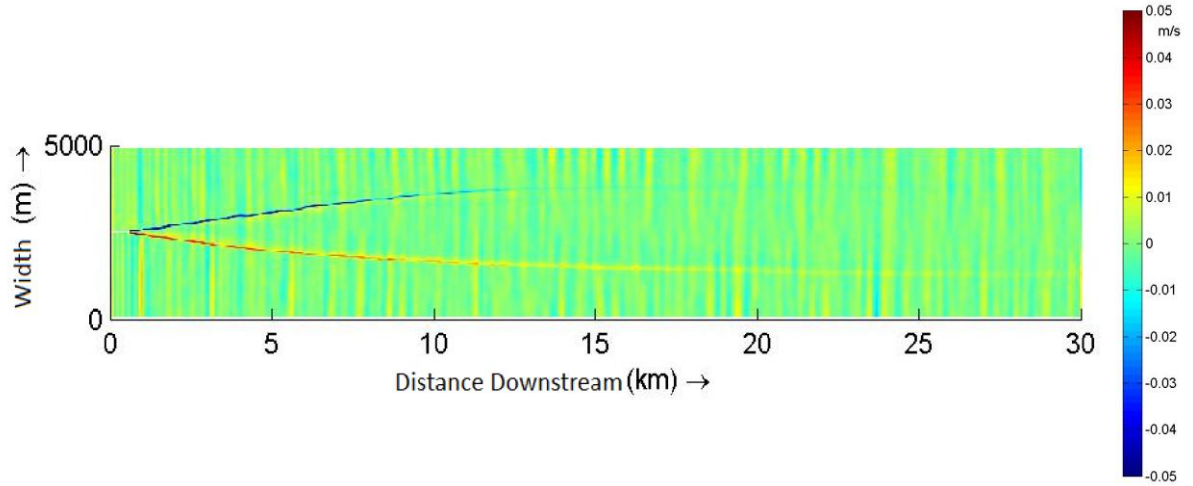

Figure 18 Vertical velocities in the middle layer.

In Figure 19 the density and the velocity in downstream direction are plotted for a longitudinal slice through the middle of the computational domain (starting directly on the lee side of the end of the dry points). Comparing the velocity and density profiles it seems that the water closer to the surface is accelerated. This acceleration causes the water to require a smaller conveyance area and therefore the interface between the waters from the two tributaries moves upwards. In Figure 20 the velocities at several depths are plotted. It is clear that close to the surface the water constantly accelerates which does not happen at lower depths.

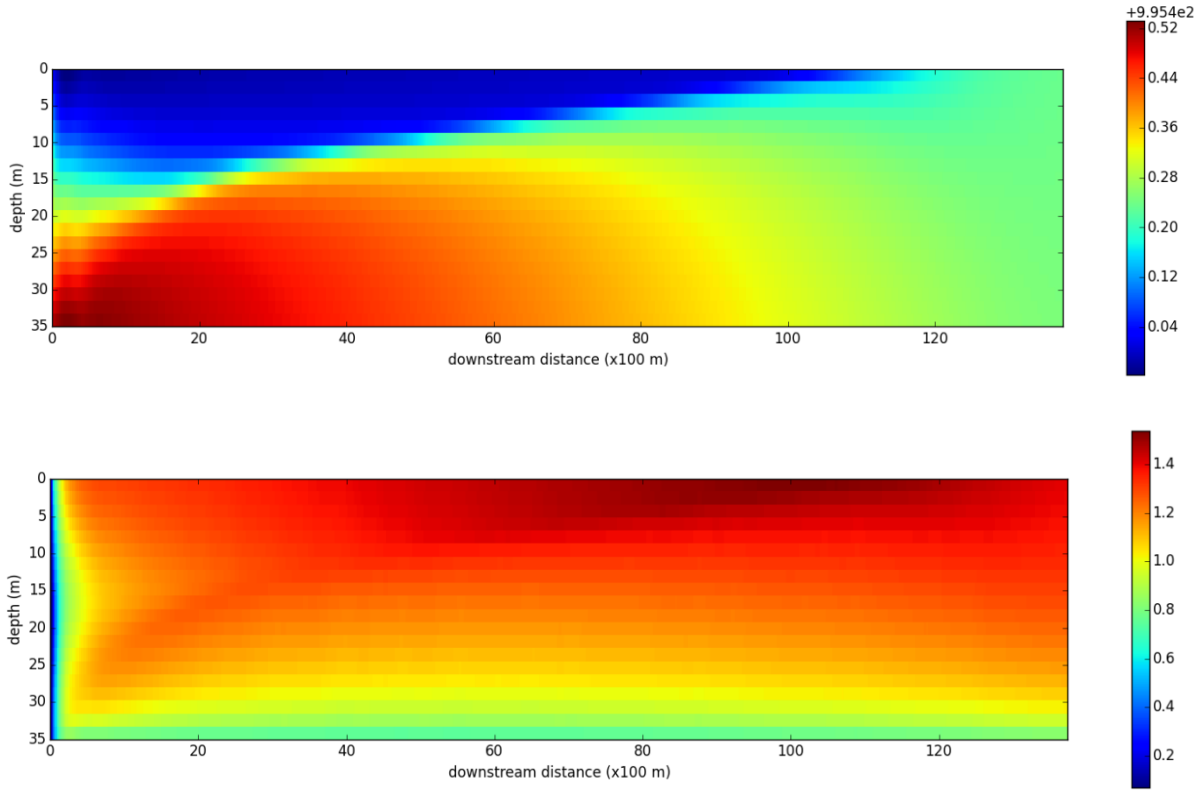

Figure 19 The density (kg/m^3) (top figure) and velocity in downstream direction (m/s) (bottom figure) for a slice through the middle of the computational domain downstream of the confluence apex.

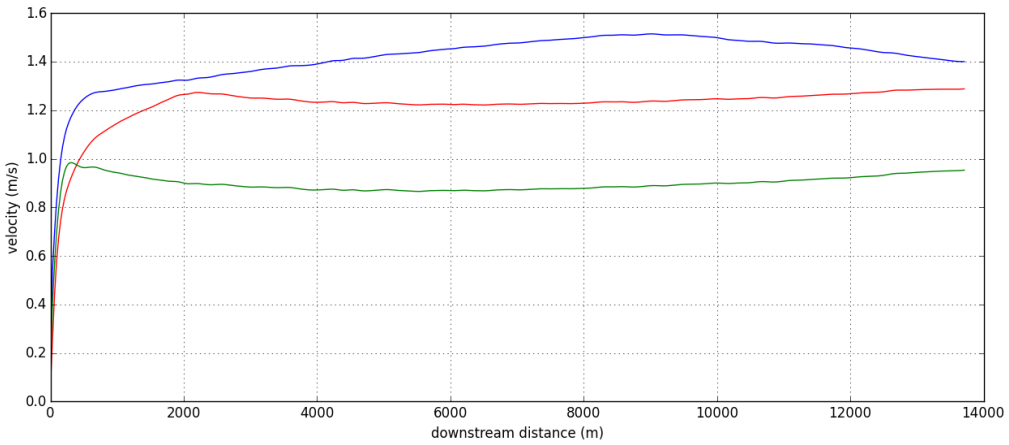

Figure 20 Velocities in downstream direction as a function of downstream direction for the layer below the top layer (blue), the middle layer (red) and the layer above the bottom layer (green).

This acceleration and upwards movement of the interface can be explained, using the two-layer model (paragraph 2.6).

It can be shown that if the flow is stationary, the equations for mass balance (2.4 and 2.5) reduce to:

$$d_1 u_1 = q_1 \quad \& \quad d_2 u_2 = q_2 \qquad (4.1)$$

Assuming a stationary flow and no wind, it can be shown that the equation for momentum balance for the top layer (2.6) reduces to:

$$u_1 \frac{\partial u_1}{\partial x} + g \frac{\partial}{\partial x}(h_b + d_1 + d_2) = \frac{s_s}{\rho_1 d_1} \qquad (4.2)$$

The second term of equation 4.2 can be simplified to gi, where i is the water level slope. We can now see that if the water level slope is large compared to the shear stress between the two layers, the

water in the top layer accelerates. Using Eq. 4.1 we can see that the top layer should then become thinner.

If overall the river is not accelerating, the acceleration due to the water level slope equals the deceleration due to the bed friction. If the shear between the two water layers is less than the shear due to bottom friction, the top layer will accelerate. If the water level slope and bed level slope are approximately equal and if the water in the top layer is not already going a lot faster than the water in the bottom layer, the top layer will accelerate. This thus also explains why the interface moves upwards in our model runs, see also Figure 5.

For this process to occur bed friction is a necessity. The less bed friction the longer it takes for the interface to reach the surface (and without friction this distance is infinite). With a lot of friction this occurs more upstream. For this process to occur in smaller confluences the friction should likely be higher. If this is not the case it is very likely that other processes like curvature induced flow have stopped this process prematurely.

The shear stress is very dependent on the velocity difference. The shear stress decelerates the faster moving water and accelerates the slower moving water. The magnitude of the shear stress depends on the velocity difference between the two waters. It is therefore easy to imagine that a velocity difference between the two tributaries has a significant influence in how fast the horizontal part of the interface moves upwards.

In Figure 21 the shape of the interface between the dense and light water is projected. Heavy water flows underneath the lighter water and lighter water over heavier water. The interface between these two waters moves upwards in downstream direction.

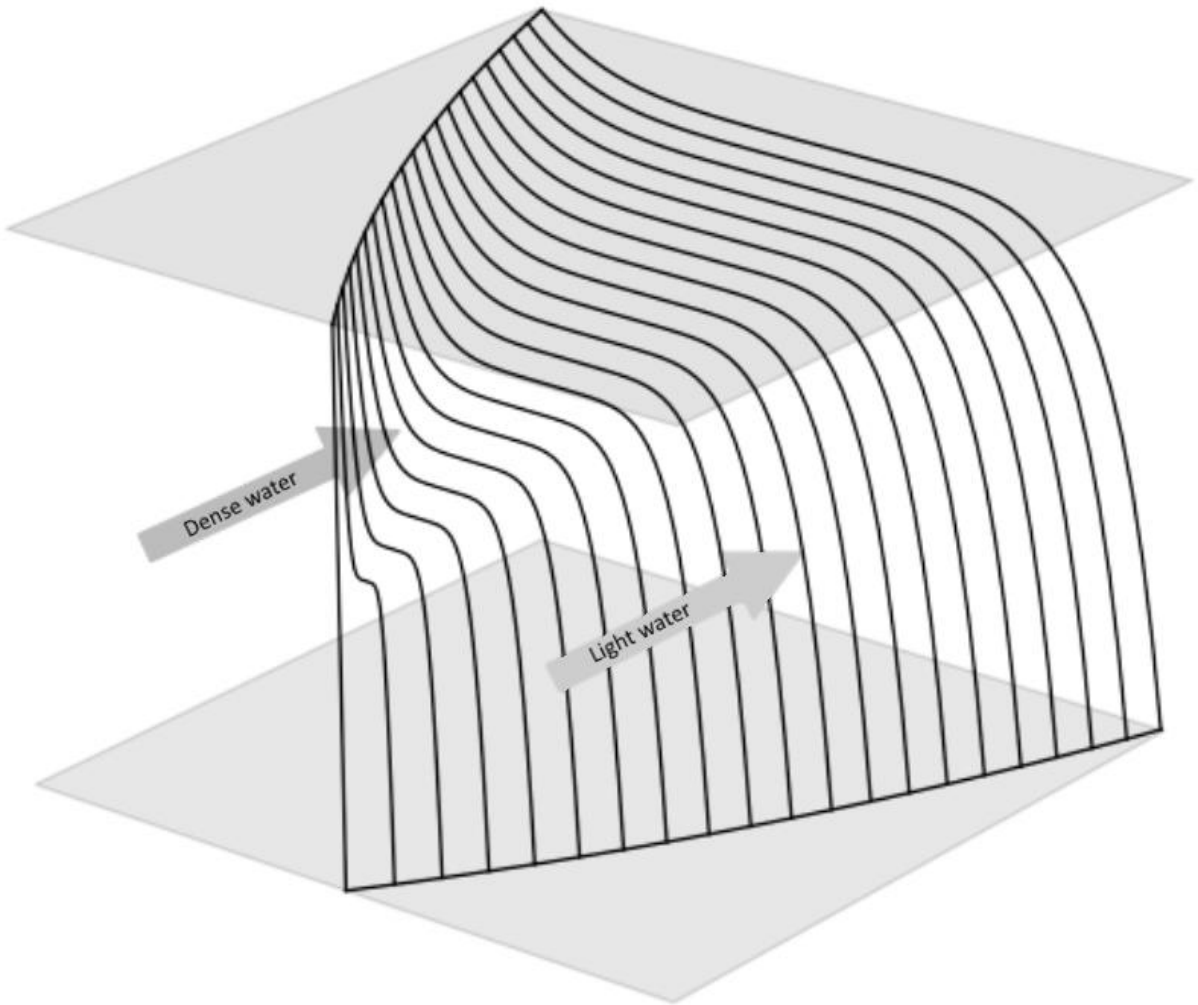

Figure 21 Shape of the interface between dense and light water. The arrows indicate the downstream direction and on which side the dense and light water enters the confluence area. The two planes indicate the water surface and bed. The vertical line is located at the confluence apex.

Effect of the changed parameters

It was already said that the models used had an aspect ratio of over 100. Different rivers have different aspect ratios. Thus the first parameter that was changed was the width of the computational domain.

It was found that the width of the river downstream of the confluence had little impact on the overturning or the amount of overturning. That is, until the river becomes so narrow that the area in which one of the waters is located above or below the other reaches a bank. In that case heavy water could well up (similar to how Biron et al. [1996] described it) or light water could well down. This is shown in Figure 22 where the river was too narrow for the dense water welling up at the surface shown in Figure 14 to occur. This can be compared to the end of a lock exchange experiment when one of the density currents reaches the end of the flume.

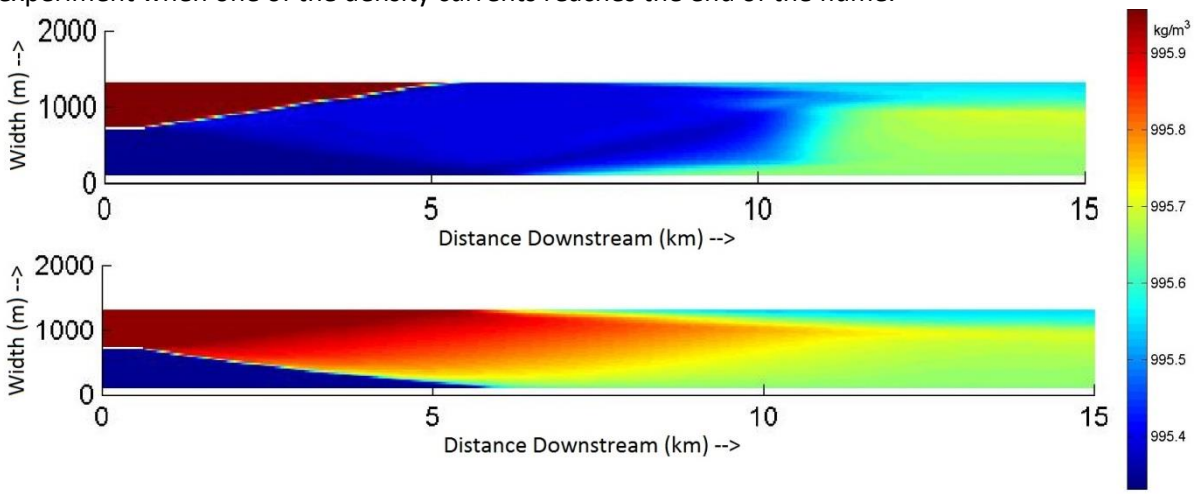

Figure 22 Densities in the top and bottom layer in a case the width becomes restrictive.

Also the influence of the bed level gradient was investigated, which seemed to have no significant influence.

The base version of the model was run with each of the available turbulence closure models: constant, k-L and algebraic [Deltares, 2014] in addition to the default turbulence closure model (k-ε) which was used in all other model runs. Of these runs only the run using the constant turbulence closure model did not show the phenomenon shown in Figure 14.

The difference between this turbulence closure model and the others is that it does not make use of the eddy viscosity concept of Prandtl [1945] and Kolmogorov [1942] and that it has a parabolic vertical velocity profile (opposed to logarithmic). It is expected that because of this in the constant eddy viscosity model the shear stress between the dense and light water is not well represented. As a result the interface does not move upwards when using the constant eddy viscosity model.

The algebraic and k-L closure models both showed similar density plots as the k-ε model. The phenomenon shown in Figure 14 occurred more upstream however. With the k-L turbulence model the location where this occurred was about the same as in the algebraic model.

Figure 23 shows that all of the other investigated parameters have an influence in the amount of overturning occurring at a certain cross-section. It seems that in all cases initially the overturning increases approximately linearly with downstream distance, which is in accordance with the theory.

In Figure 23 we can see that only initially the increase in amount of overturning is linear and that it starts reducing quite soon after the confluence apex. This can be understood by using equation 2.3. It states that the celerity of the density current is dependent on its height, which, in this case, does not remain constant. We have two density currents here (one heavy water current protruding into light water at the bottom and one light water current protruding into heavy water at the surface). At the beginning the heights of both density currents are about half the depth, whereas

further downstream the density current at the bottom grows higher and the one at the surface becomes smaller in equal measure. Thus in the beginning: $\frac{dAoO}{dx} \propto \sqrt{h_{c1}} + \sqrt{h_{c2}} = \sqrt{\frac{1}{2}h} + \sqrt{\frac{1}{2}h} = \sqrt{2h}$ whereas more downstream $\frac{dAoO}{dx} \propto \sqrt{\frac{1}{2}h + \Delta h_c} + \sqrt{\frac{1}{2}h - \Delta h_c}$ and in the extreme case where Δh_c=½h this can become: $\frac{dAoO}{dx} \propto \sqrt{h} + \sqrt{0} = \sqrt{h}$. The rate in which the amount of overturning increases can thus reduce up to a factor $\frac{\sqrt{2h}}{\sqrt{h}} = \sqrt{2}$. The shape of $\frac{dAoO}{dx} \propto \sqrt{\frac{1}{2}h + \Delta h_c} + \sqrt{\frac{1}{2}h - \Delta h_c}$ (changing Δh_c) is in agreement with Figure 23. At first the change of Δh_c has little influence but the more it has changed the more influence it will have.

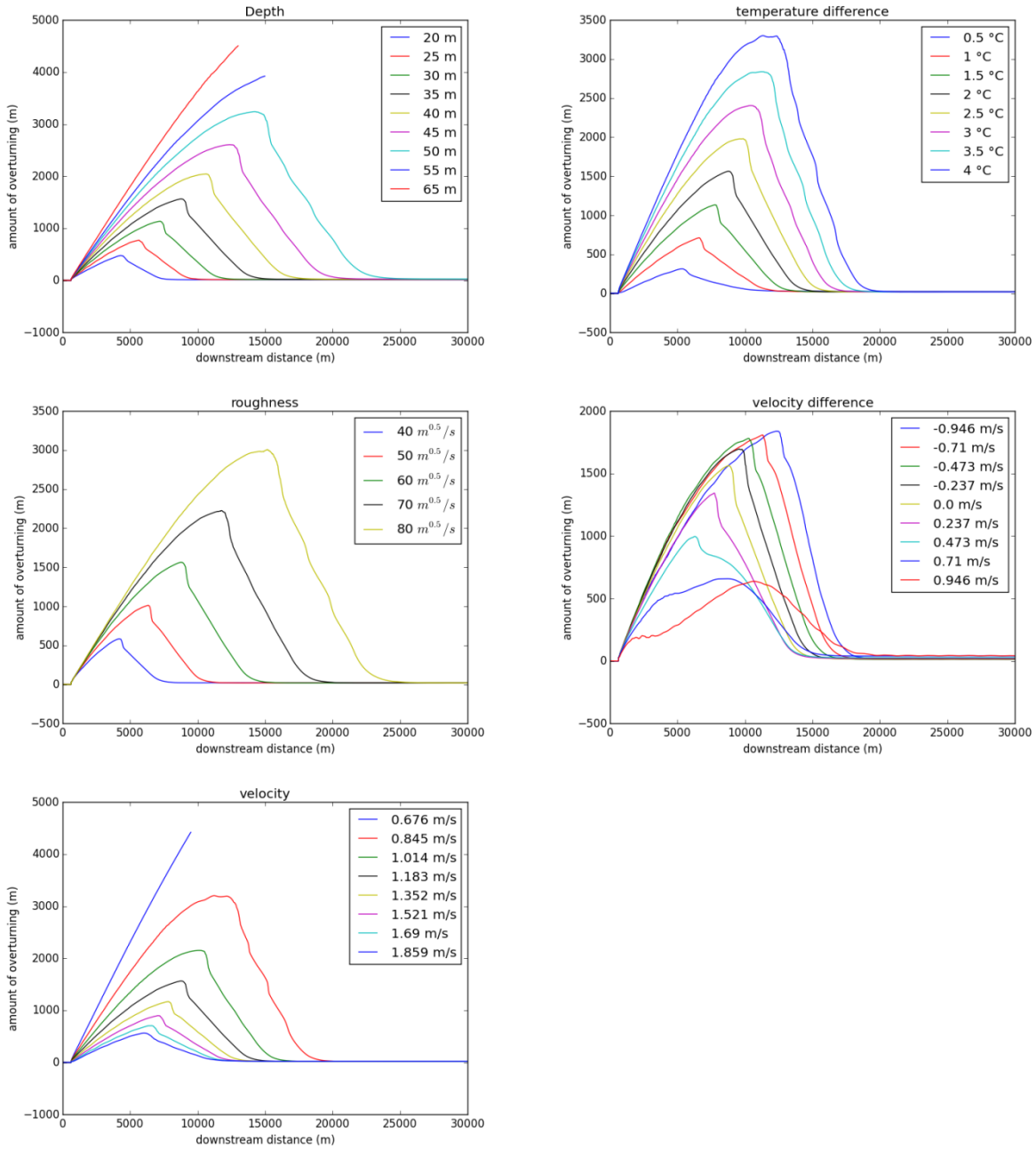

Figure 23 The amount of overturning as a function of the downstream distance for various cases. From left to right and top to bottom: depths, temperature differences, roughness, velocity differences, velocities.

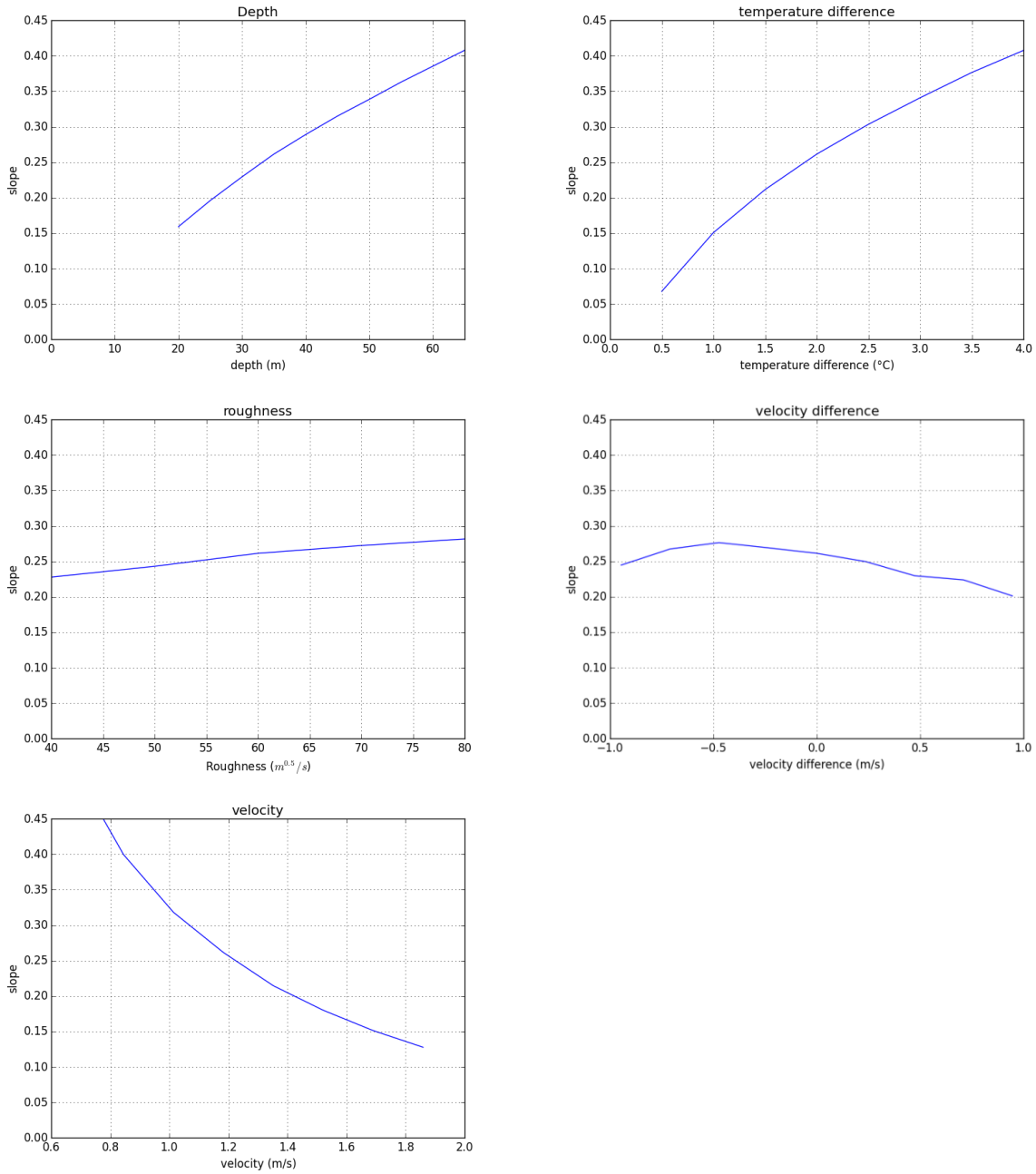

Figure 24 The slope of the initial part of the overturning as a function of the changed parameters. From left to right and top to bottom: depths, temperature differences, roughness, velocity differences, velocities. The vertical scale is kept the same throughout the figures.

Using least squares fitting it is easy to approximate the slope of the initial linear growth of the amount of overturning. For each of the parameters the slopes are plotted in Figure 24. From this figure we can conclude that for parameter sets which can occur in real rivers the velocity difference and roughness have a small influence compared to the velocity, depth and temperature difference.

This is what we would expect as it was found by Benjamin [1968] that the depth and density difference influenced the celerity of a density current. The velocity additionally advects everything downstream and therefore also has an influence. The velocity difference has no effect on the mean advection; only on the difference in advection between the high and low density part.

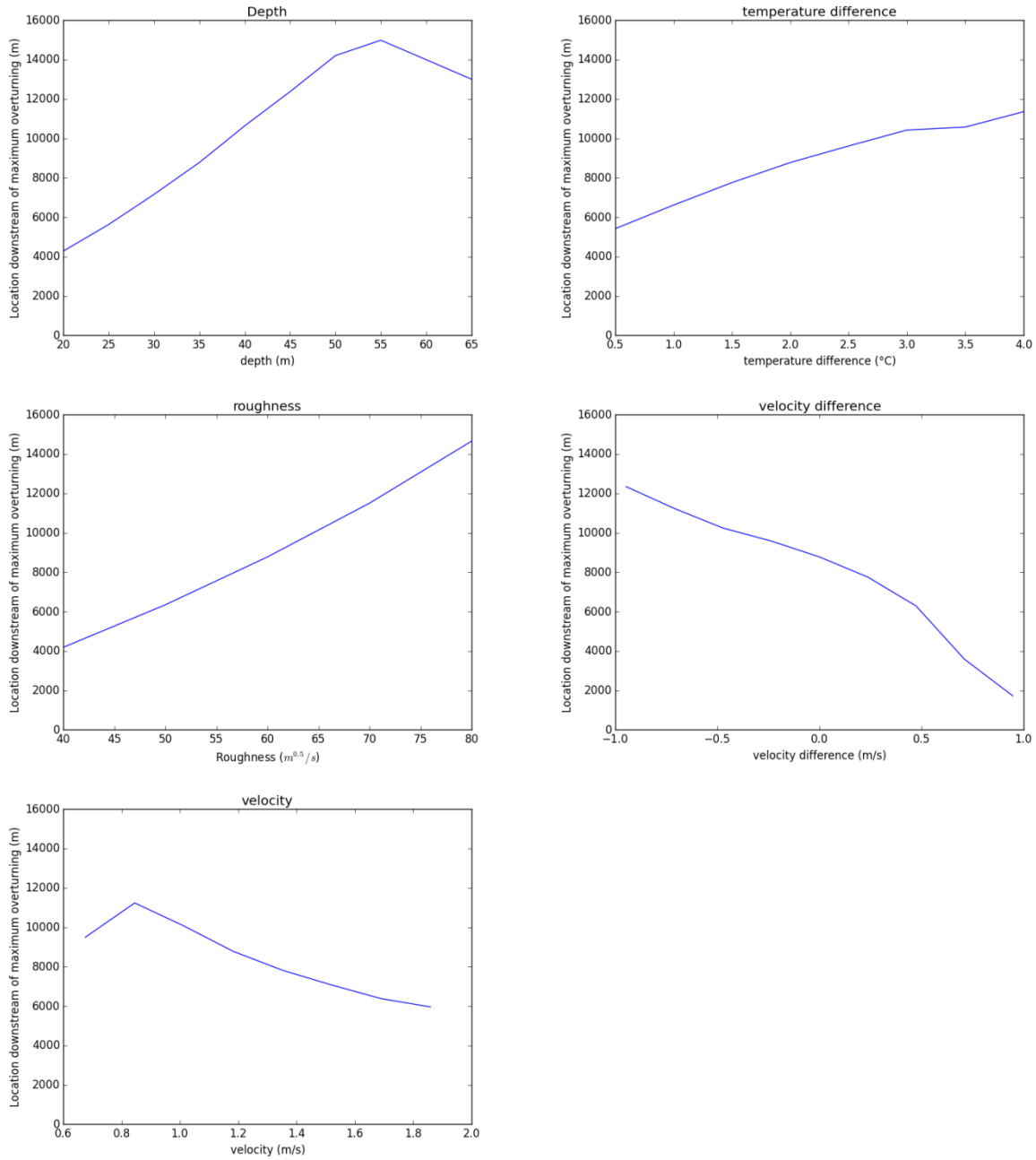

Figure 25 The distance downstream of the confluence apex of the location of maximum overturning as a function of the changed parameters. From left to right and top to bottom: depths, temperature differences, roughness, velocity differences, velocities. The vertical scale is kept the same throughout the figures. The sudden drop at the higher depths and lower velocities can be explained by the fact that one of the density currents reached the bank before the maximum overturning could occur.

Actually if we look at Figure 23 we can see that the slope does not change at all with roughness or velocity ratio. These parameters only have an effect on how far downstream the overturning stops.

Figure 24 also shows that the amount of overturning becomes infinite with a velocity of 0. In that case there is no difference with the normal lock exchange and the water would have an infinite time to overturn before it reaches a point downstream of the confluence. The overturning will thus become infinite. This physically means that water from one tributary can end up upstream in the other tributary, as seen by Lyubimova [2014] in a confluence with very small velocities.

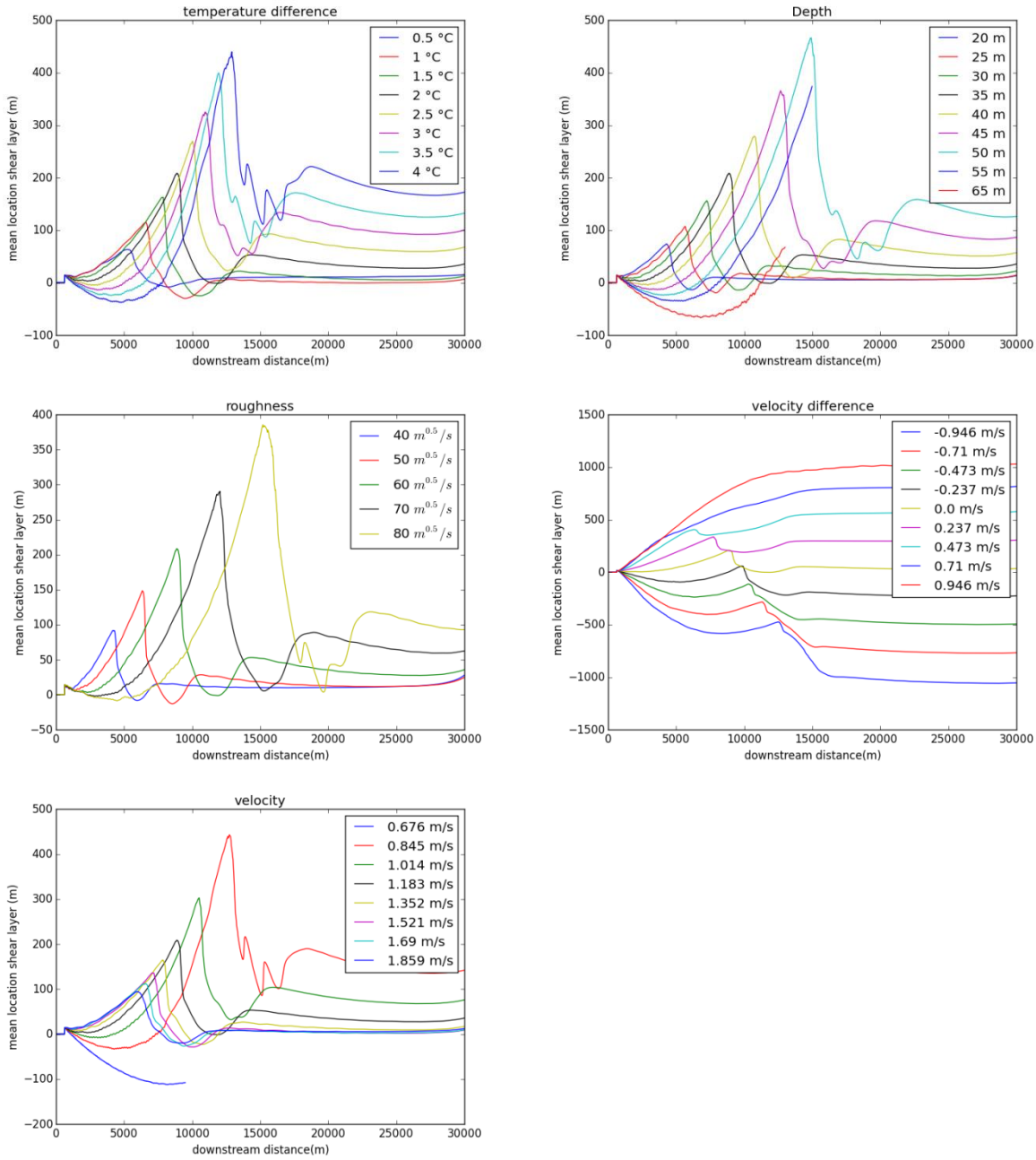

Figure 26 Mean location of the shear layer as a function of downstream distance for each of the paratemers. From left to right and top to bottom: depths, temperature differences, roughness, velocity differences, velocities.

In Figure 25 the downstream distance from the confluence apex to the location where the maximum overturning occurs is plotted against several parameters. We can see that also some parameters which have little influence on how fast the overturning occurs have a large impact on where the maximum overturning is located. At the point of maximum overturning the horizontal interface reaches the surface. As noted before both the bed roughness and velocity difference between the two tributaries are of major importance in this process even though they have little influence on the speed of overturning.

It is not enough to know how much overturning occurs in order to find out where water from each tributary ends up (or to find out if it reaches a specific location, e.g. the bank). The mean location of the shear layer should also be known. Figure 26 shows the mean location of the shear layer (right in the middle of the points where the mean density hits the surface and bottom) for each of the parameters. In the plots 0 m means the middle of the channel and if no density differences or

velocity differences would be present that is where the shear layer should be. Clearly the density differences cause the mean location of the shear layer (note: not the depth averaged location) to shift across the river. Generally speaking the maximum deviation of the mean location is about $1/7^{th}$ of the maximum amount of overturning, only the roughness seems to have a (small) impact on this number.

The mean location of the shear layer tends to go towards the side of the heavier water. The depth averaged location of the shear layer thus stays approximately in the middle of the river channel (because the heavier water takes up a larger portion of the depth).

We can see in Figure 26 that the graphs of mean location of the shear layer do not have the same shape as those of the amount of overturning. Where the graphs of the amount of overturning (Figure 23) are concave, those of the mean location of the shear layer are convex.

Due to the way the mean location is defined here, it has a great dependency on the celerity difference between the two density currents. Actually the difference in mean location between two points can be completely determined by the velocities of the density currents. The larger the celerity difference is, the faster the mean location will change. As was described earlier, the celerity of the two density currents changes as we go in downstream direction due to the lower density current growing higher. Thus the celerity difference also grows in downstream direction and the mean location will change more rapidly further away from the confluence apex.

The main exception is the velocity difference. This is because as is already known the shear layer will move to the slower moving fluid [Kirkil, 2015]. The figures suggest that the effect of the density differences and the effect of the velocity differences can be added to find the mean location of the shear layer.

Using a non-dimensional parameter as a predictor for the amount of overturning

The depth and density difference thus have a similar square root relation with the rate at which the amount of overturning increases. Additionally a similar graph for the velocity shows a hyperbola. This raises the question if it is possible to find a relation between the amount of overturning and these parameters.

Figure 27 shows the relationship between the amount of overturning divided by the distance from the confluence apex and the Richardson number (computed at the confluence apex). The Richardson number is the ratio between the motions due to density differences and the advection and can also be defined as the inverse of the density Froude number.

From Figure 27 it is clear that a relationship between these two parameters exists. In this figure it is however clear that all points measured about 2 km downstream of the confluence apex are above those measured about 4.5 km downstream of the confluence apex. It was already explained that the rate at which the amount of overturning increases, reduces with downstream distance. This reduction was caused by the change in h_c, which is also part of the Richardson number. This thus explains why all crosses are located above the dots.

In the figure one green dot can be seen well below the other data points. This dot was measured too far downstream. It was measured downstream of the location of maximum overturning (in the area where the AoO reduces again). Note that no points can be located above this line, but only below this line.

All data points in Figure 27 came from models using a Chézy coefficient of 60 $m^{0.5}/s$. If friction were to be reduced (a higher Chézy value) the line shifts upwards. If friction is increased the line moves downwards. It is expected that if no friction is present: AoO/x=Ri holds.

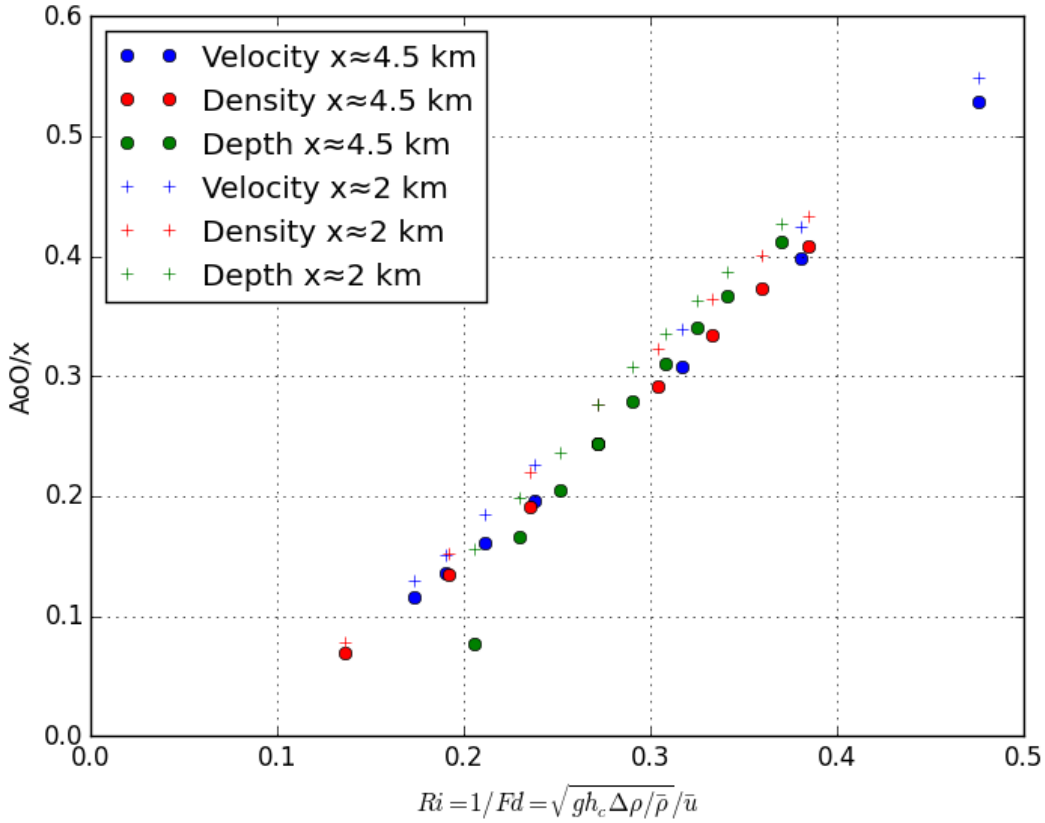

Figure 27 Graph displaying the relation between the dimensionless amount of overturning and the Richardson number. The different colours indicate how for that model the Richardson number was varied. For the dots the AoO was measured about 4.5 km downstream of the confluence apex and for the crosses they were measured about 2 km downstream of the confluence apex.

4.3 Effect on the mixing layer

In Figure 14 no clear mixing layer develops due to the trivial reason that there is no velocity difference. If we now look at Figure 28 which has an equal velocity difference and ratio as the test case for the mixing layer as shown in Figure 11, we see no large coherent structures at the surface. Some Kelvin-Helmholz instabilities are visible closer to the bottom (with length scales up to 300 m).

Instabilities generally develop as columns. Due to the motions perpendicular to the main direction of flow due to the density differences these columns can be distorted. This distortion hampers the development of the mixing layer.

This process is similar to the flow over a bottom with differing roughnesses [Vermaas et al., 2011]. In that case also a secondary circulation will develop (although the length scale is much smaller than here due to density differences) that can destroy large coherent structures. The secondary circulation in that case is probably of the smallest length scale that it is able to destroy coherent structures.

In the model run with maximum velocity differences (same as Figure 11 and Figure 28) but with half the density difference of the run of Figure 28 some instabilities could be observed at the surface (see Figure 29). These structures are however not as developed as those in Figure 11. A smaller density difference, with smaller motions in the plane perpendicular to the main direction of flow thus has a smaller effect on the development of the mixing layer. Note that in Figure 29 not only the mixing layer has changed but also the amount of overturning and the rate at which the heavy water moves upwards, both because of the change in density difference.

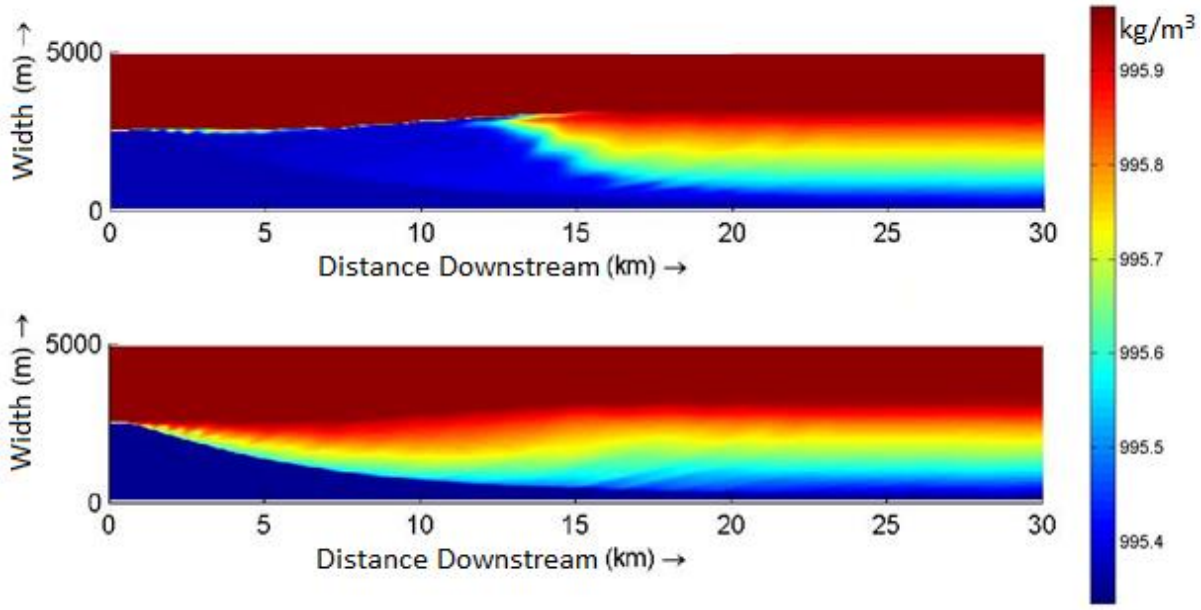

Figure 28 Water density for the top and bottom layer for the case with a velocity difference equal to that of Figure 11

A relation for when the large coherent structures occur in the mixing layer was found. Two non-dimensional parameters were used. The first one is the velocity difference divided by the mean velocity. The velocity difference is the driving force for the development of the mixing layer, the mean velocity influences how fast structures are advected downstream. The higher this number the more likely it is that coherent structures will develop.

The second parameter is again the Richardson number, which is the ratio between the motions due to density differences and the advection. The motions due to density differences hamper the development of the mixing layer. Thus the higher the Richardson number the less likely it is that a mixing layer will develop.

Figure 30 shows a diagram which shows for which combinations of these two non-dimensional parameters coherent structures can occur and for which coherent structures cannot occur. Note that if a density difference is present the development of the coherent structures in the mixing layer is always hampered to some degree. Since the coherent structures increase the length

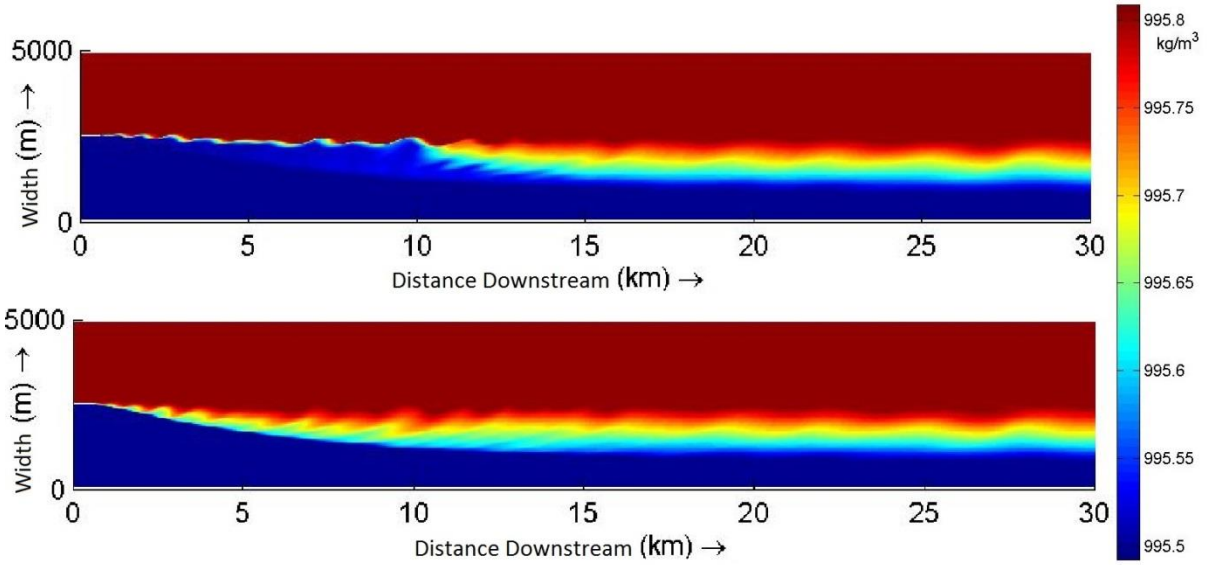

Figure 29 Water density in the top and bottom layer for the case with maximum velocity difference and half the density difference.

scale of the mixing layer this means that the mixing layer will have smaller length scales decreasing mixing. Note also that there is no clear division between when coherent structures will develop and when not. For some of the model runs coherent structures were undetectable at the surface whereas at the bottom still small Kelvin-Helmholz instabilities were visible.

As noted before Daoyi & Jirka [1198] described a stability number, S. For certain values of this stability number no instabilities and thus no coherent structures are able to develop. This stability number depends on a length scale l which is the width of the mixing layer. The width of the mixing layer however changes with downstream distance. A logical choice for the critical width of the mixing layer is that it is as wide as the water depth. If the mixing layer is namely wider than the water is deep the coherent structures need to be predominantly two-dimensional.

Using the water depth for the length scale in the stability parameter we gain the following requirement for coherent structures: $S = \frac{2c_f\bar{u}}{\Delta u} < 0.1$. This results in a horizontal line in Figure 30 of which the height is dependent on the friction. The more bed friction there is, the higher this line is located in Figure 30.

When investigating a confluence, a dot can be placed in Figure 30 which then tells if coherent structures may develop or not. This could not be done for the confluence studied by Cook & Richmond [2004], since not all required parameters are available. The confluence studied by Lyubimova et al. [2014] is of the chart; the velocity in this confluence is so low that the Richardson number equals roughly 3. For such a high Richardson number density currents are able to move upstream which was also observed by Lyubimova et al. [2004].

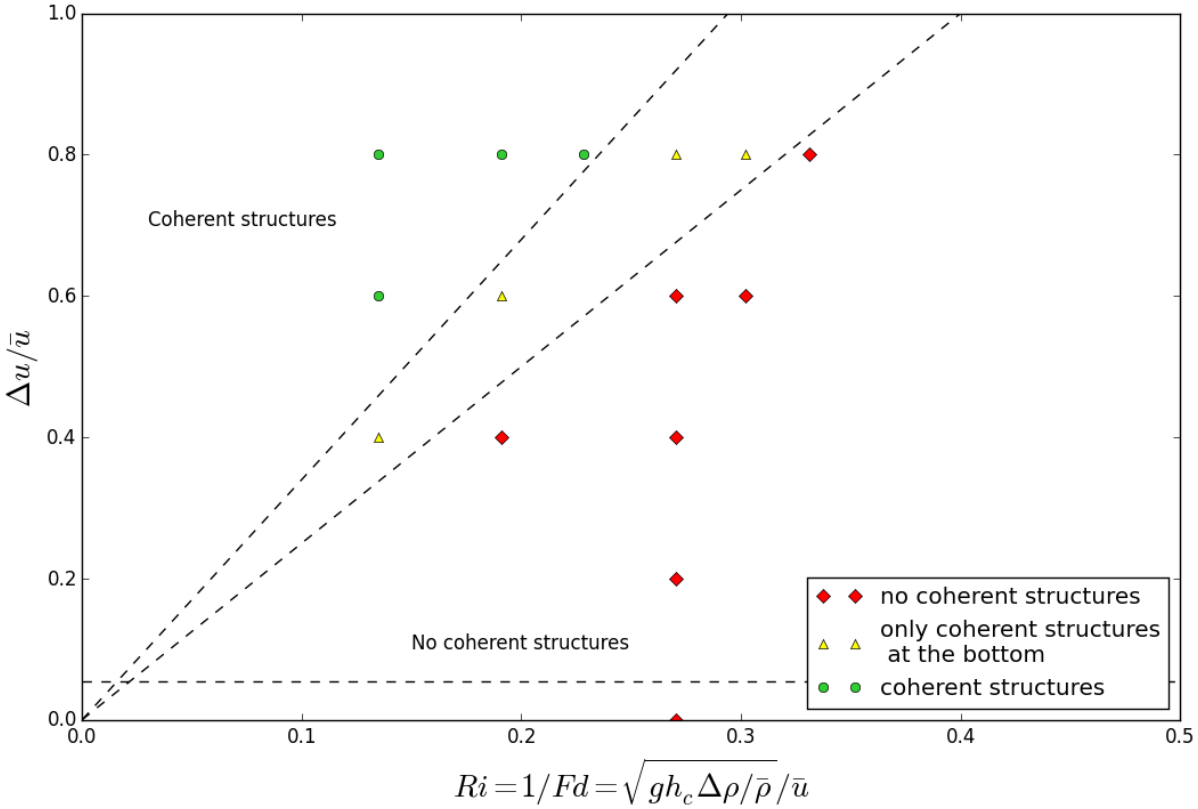

Figure 30 Diagram showing under which conditions a mixing layer can and cannot develop. The green, yellow and red dots correspond with model runs where a mixing layer was present, only present at the bottom or not present at all respectively.

Both non-dimensional parameters used, have the velocity as the denominator. It should thus be possible to use only one non-dimensional parameter:

$$\frac{\Delta u}{\sqrt{g\frac{\Delta\rho}{\bar{\rho}}h_c}}$$

The slopes of the lines which divide the diagram in areas are then the values for this non-dimensional parameter where the type of flow in the confluence changes:

$$\frac{\Delta u}{\sqrt{g\frac{\Delta\rho}{\bar{\rho}}h_c}} > 3.4 \qquad Coherent\ structures$$

$$\frac{\Delta u}{\sqrt{g\frac{\Delta\rho}{\bar{\rho}}h_c}} < 2.4 \qquad No\ coherent\ structures$$

This non-dimensional parameter is the ratio of the velocity difference, which is the driving force for the mixing layer, and the motions due to density differences hampering the development of the mixing layer. These values give a good first approximation if coherent structures can develop or not, however the values are based on a limited set of model runs; more model runs could increase the accuracy of these values.

The lines in Figure 30 divide the area into areas where coherent structures can or cannot develop. These lines are based on different ways of hampering the development of these structures. The horizontal line indicates hampering of the coherent structures due to friction and the diagonal ones due to motion perpendicular to the main direction of flow. Friction might also have an indirect influence on the development of coherent structures as it could influence the motion perpendicular to the main flow direction. It might also be possible that both processes alone are not able to stop the development of coherent structures but still structures will not develop because both of the processes together hamper the structures enough to not develop.

At various dots in Figure 30 two model runs are located. These model runs than have a differing depth and density difference. In none of these cases another classification for the mixing layer (coherent structures, only coherent structures at the bottom, no coherent structures) was needed. This thus seems to validate Figure 30.

However, at certain points where two model runs were run it was clear that the coherent structures were more developed in one of the runs. The Richardson number is dependent on the height of a density current, it was assumed here that that is half the depth. Initially this was also the case but as was noted before the interface between the two waters moved upwards thus changing h_c. It is expected that this causes the small differences between the model runs with similar non-dimensional parameters. Since the speed at which the interface moves upwards is not yet adequately investigated no better approximation can be given.

4.4 Aerial photographs

An overturning of the shear layer due to density differences has been identified. Also the heaving of the lower, denser water has been identified. Ultimately this denser water emerges at the surface. These processes have been identified using numerical modelling. The next step is to see if this flow situation can also occur in real-life confluences. For this end aerial photographs and satellite imagery were used. In Figure 31 and Figure 32 photographs with very similar flow structures as seen in for instance Figure 14 and Figure 28 are shown.

Figure 31 shows the confluence of the Irrawaddy and Chindwin rivers. The colour of the Chindwin (lighter coloured in the figure) indicates that the Chindwin has a higher density. The colour is likely influenced by the sediments it carries. Just downstream of the confluence the Chindwin takes up a wider part of the river branch (at the surface). More downstream, even though minor amounts of Irrawaddy water are discharged through small branches, the width where Irrawaddy water is present grows (at the surface). This is most likely because the Irrawaddy water is lighter and flows over the Chindwin water. A little further downstream the width where the Irrawaddy water is present suddenly decreases again, most likely due to the effect of the horizontal part of the separation layer reaching the surface.

Figure 32 shows two photographs of the Niger-Benue confluence in Nigeria. Similar to the Irrawaddy – Chindwin confluence, the lighter coloured water (Niger River) is assumed to have a

higher density. In the photograph taken in 2011 we see a similar distribution of the colours as in the Irrawaddy Chindwin, where first the lighter river increasingly takes up a larger width at the surface and more downstream the heavier river increasingly takes up a larger portion of the width again (at the surface).

Figure 31 Photograph taken on 26 Oct 2009 of the Irrawaddy-Chindwin confluence (Myanmar), source DigitalGlobe

The photograph taken in 2005 also clearly shows an area where the width at the surface of the heavier water is growing rapidly. The part more upstream of this where the lighter water takes up a larger part of the width is not very well visible on this photograph. What we do see however is a clear mixing layer developing between the two tributaries starting from the confluence apex. This indicates a (significant) velocity difference between the two tributaries. The absence of the lighter water taking up a larger portion of the width at the surface can be explained if the Niger River would flow faster than the Benue River. In that case the entire shear layer would be pushed towards the Benue side and therefore reduces the portion of the width where Benue water is present throughout the water column (so also at the surface). The mixing layer of course also indicates that the density difference is not too large (see Figure 30).

Figure 33 shows the confluence of the Rhône and Arve rivers. On this photograph we can see the Arve river (lighter coloured and denser) diving under the Rhône river. A little downstream of the confluence apex Arve water is upwelling near the bank of the Rhône. This is similar to what we saw in Figure 22 for a narrow river.

These photographs seem to validate that the processes of heavy water upwelling due to the heaving of the separation layer between the two waters or near the bank due to a width restriction, can occur in nature. Unfortunately at all of these confluences not enough data is available to place them in Figure 30.

Figure 32 Photographs taken on 5 Dec 2011 (left) and 21 Dec 2005 (right) of the Niger-Benue confluence (Nigeria), source DigitalGlobe

Figure 33 Aerial photograph of the confluence of the Rhône and Arve, near Geneva (Switzerland). Photo taken on 1 July 2009. Source: Google Earth.

4.5 The Rio Negro – Solimões confluence

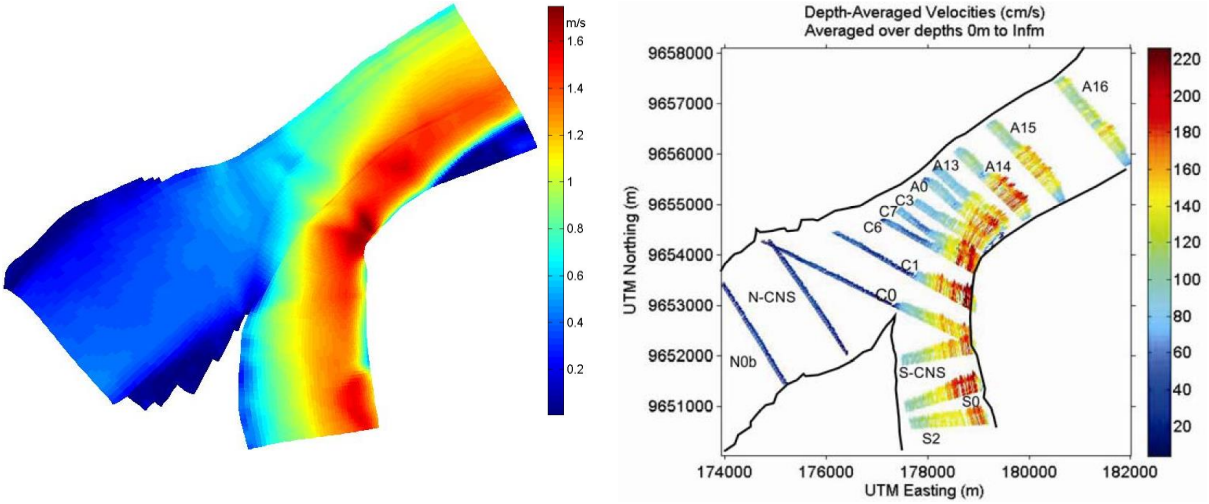

Figure 34 The depth averaged velocities following from the low flow case of the model (left) and from the measurements done by Trevethan et al. [2015b] (right), right after Trevethan et al. [2015b]

To check if the numerical model of the Rio Negro – Solimões confluence functions well the velocity profiles (of low flow case) were compared to the velocity profiles measured by Trevethan [2015b]. In Figure 34 the measurements of the depth averaged velocity done by Trevethan et al. [2015b] and the depth averaged velocities following from the model are shown side by side. A clear correlation seems to exist. Both the velocity profiles and the velocity magnitudes seem to correspond quite well. The flow discharges used in the numerical model were not identical to those during the measurements, although the model and the measured values differ only slightly. During the measurements of Trevethan et al. [2015b] the discharge of the Solimões was about 5% higher than the discharge used in the model, which explains the differences in velocities. The correspondence is quite remarkable considering the fact that the model is schematized and uncalibrated.

The model for the confluence area of the Rio Negro and the Solimões showed a clear overturning of the shear layer, see Figure 35. As noted before many different settings were used for this model, however none of these showed an overturning due to the bed discordance. Therefore it assumed that the bed discordance does not play a role in the overturning for this confluence.

There can be two reasons why we may not see an effect of the bed discordance in this case: 1. the bed discordance doesn't have an influence or 2. the model cannot solve the effect of the bed discordance.

Biron et al. [2004] used a numerical model which calculated/simulated this process for very small natural and laboratory confluences. In their model a grid was used with smaller grid cells compared to the bed discordance height than the grid cells that were used in our model.

In a thought experiment we can investigate a hypothetical confluence in which one tributary has a bed level equal to the downstream bed level and the other tributary has a higher bed level. If the influence of the tributary with the same bed level is reduced, then the confluence would slowly turn into a river with a classical backwards facing step.

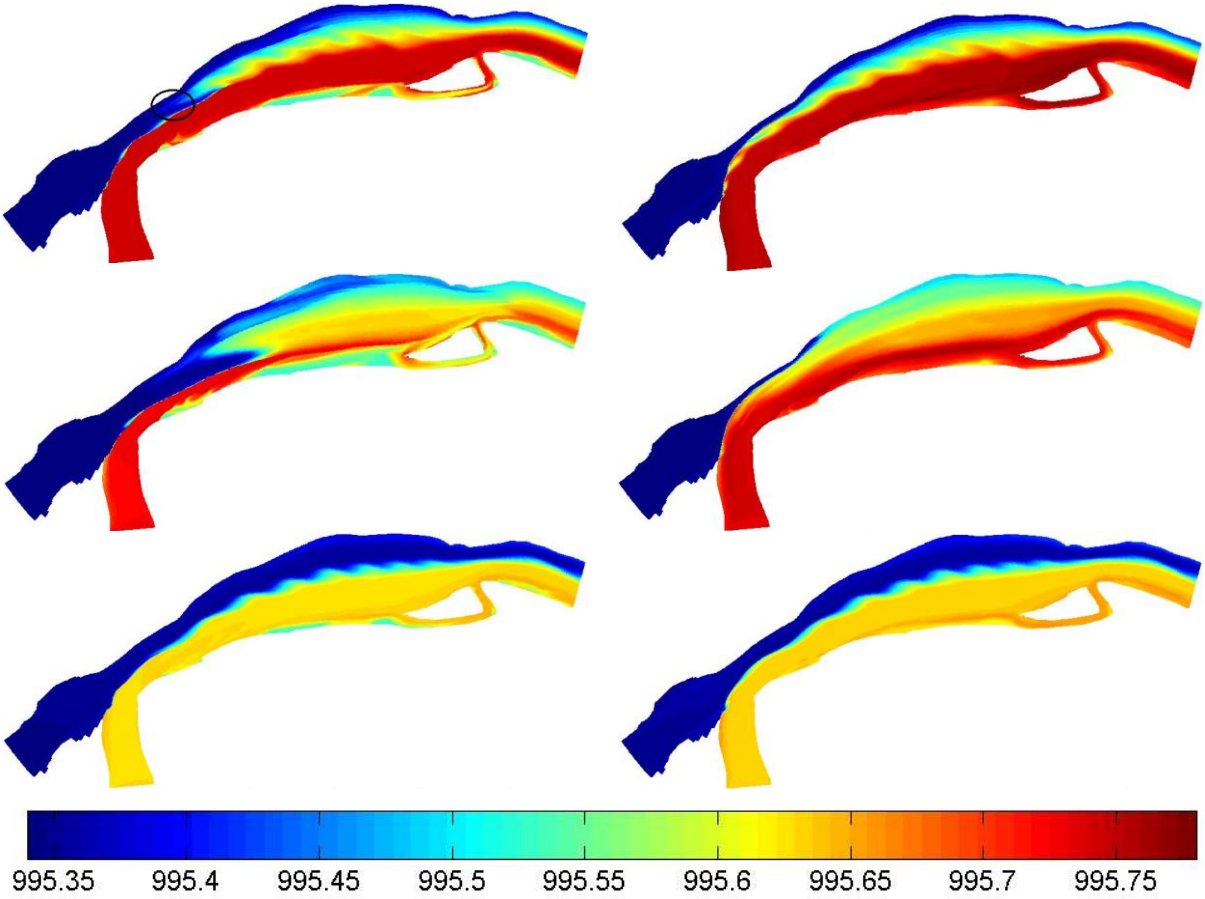

Figure 35 Densities (kg/m^3) from the Rio Negro-Solimões model. Highest momentum ratio (top), Low flow (middle) and High flow (bottom). Top layer (left) and bottom layer (right). The approximate location of Figure 37 is indicated in the top left plot.

It is known that behind a (sharp) backwards facing step an eddy will develop. The length of this eddy is several times the step height and can be seen as a typical horizontal length scale for the backwards facing step problem.

It thus seems likely that the effect of the bed discordance can only be solved if the eddy behind a backwards facing step of the same height as the bed discordance can be solved. To solve for such an eddy the grid cells should be small enough, which in our model is not the case.

If we would use a similar grid cell size to step height ratio as Biron et al. [2004] used in our model, we would require several billion grid cells which is computationally very demanding. Also we would basically be doing a LES for the flow domain whereas this is a problem which should be solvable with Reynolds Averaged Navier-Stokes (RANS).

This thought experiment tells us something else as well. We saw that the horizontal length scale of an eddy forming behind a backwards facing step or for the effect of the bed discordance was several times the step height. This horizontal length scale is significantly smaller than the width of the river, or the length scale over which overturning can occur. Considering the large difference between these two length scales it seems logical that the influence of the bed discordance on the overturning of the shear layer is small. Therefore it is assumed that only the density difference causes the overturning of the shear layer for the Rio Negro – Solimões confluence.

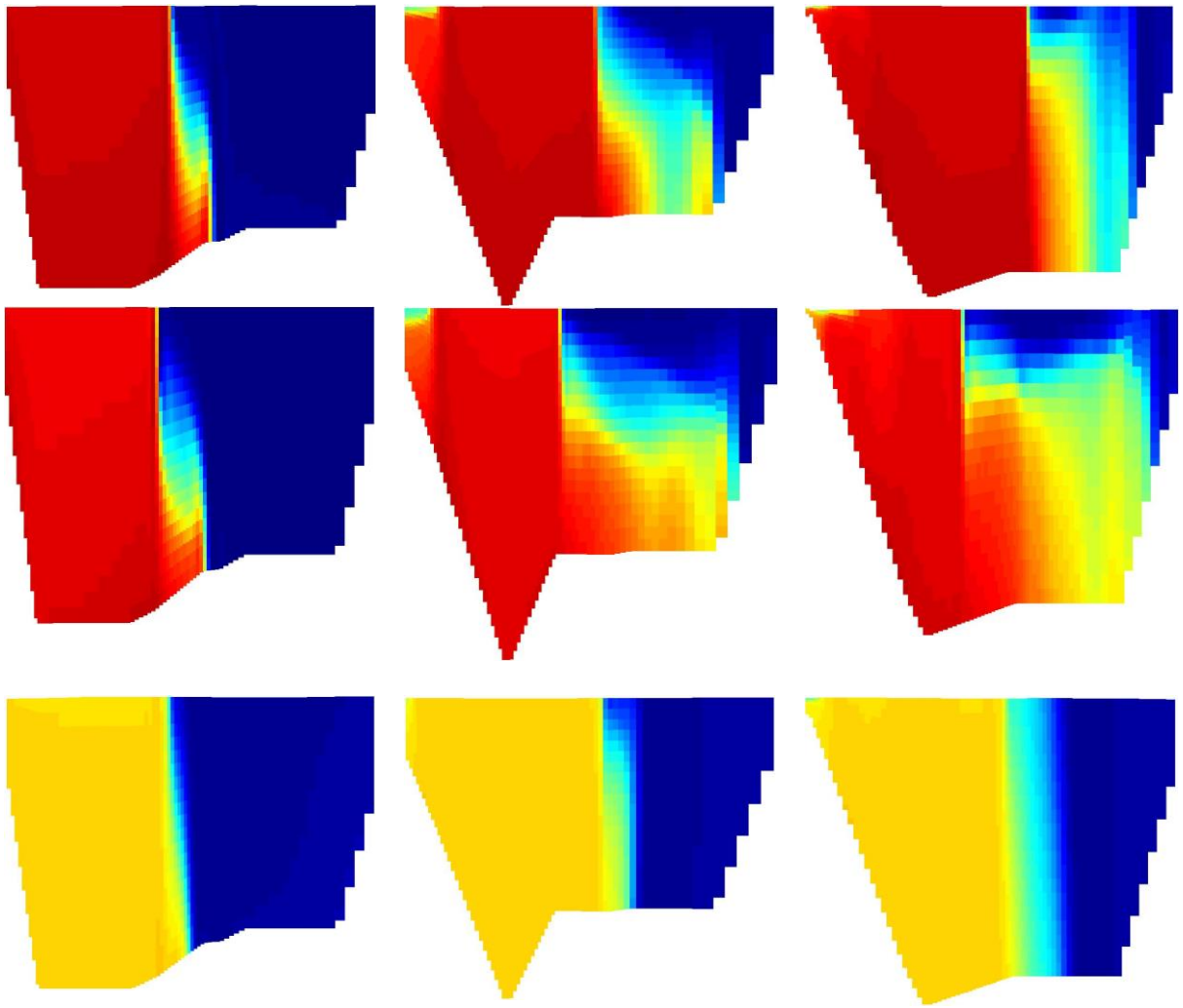

Figure 36 Densities in several cross-sections (indicated in Figure 10) for the highest momentum ratio (top), low flow (middle) and high flow (bottom), the same colours are used as in Figure 35. More to the right is more downstream.

Figure 36 shows cross sections at several locations downstream of the confluence. It is clear that a significant overturning is occurring. The overturning reached values larger than 500 m! Comparing the overturning for the differing flow stages it is clear that during low flow stages the overturning is much more pronounced than during high flow stages, which is in accordance with the described theory.

In several aerial photographs of the Rio Negro – Solimões confluence turbulent boils of Solimões water inside Rio Negro water were found. These boils occurred at nearly identical locations, see Figure 37. Due to their near constant locations they are believed to be the kind of boils that develop behind bed disturbances. These bed disturbances would then be stationary in time and are therefore likely not of sedimentary origin (for instance large boulders or a sunken ship etc.).

A more thorough investigation of the boils on the aerial photographs showed that the boils only occurred in specific months and therefore under specific flow conditions. Unfortunately not in each month aerial photographs are available, but the general tendency is that boils only occur during months of low water discharge, see Table 2 and Figure 9.

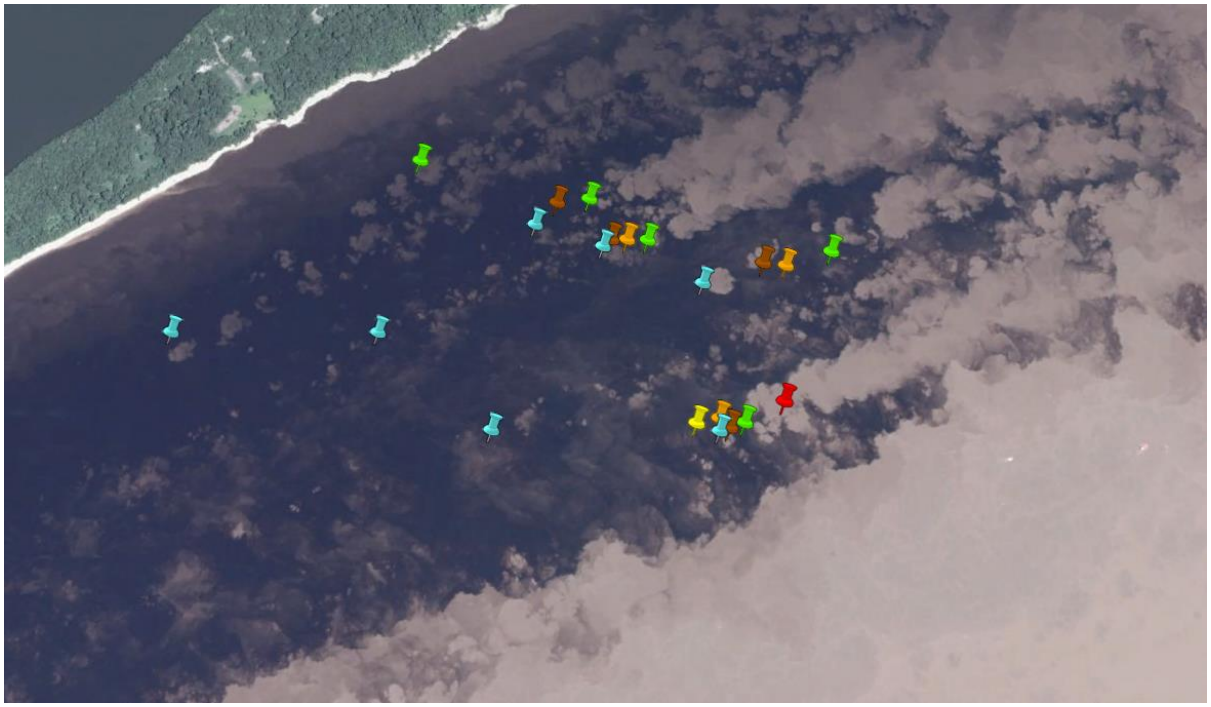

Figure 37 Aerial photograph of boils with Solimões water on the Negro side of the river, 30 Nov 2014, source: DigitalGlobe. The markers show the most upstream boil spotted on a certain photograph, the different colours denote different years, the cyan markers pertain to 30 Nov 2014. The location of this photograph is indicated in Figure 35.

A similar analysis was performed on LANDSAT imagery of which the results can be found in appendix B. The results are consistent with the findings of the aerial photographs. However it should be noted that the LANDSAT imagery is of lower quality than the aerial photographs and therefore the analysis of the LANDSAT images is more prone to errors.

Boils can transport (white) Solimões water upwards only if this water is available at the bottom. The most likely explanation for these boils occurring only during specific months is therefore that only if the velocity is low enough Solimões water is present at the bottom. The low flow and highest momentum ratio cases of the models would be at a time that boils would occur, whereas during high flow they would not. The models are in agreement with this hypothesis. In appendix D. the effect of vertical stratification of the water column on the occurrence of boils is briefly discussed.

In the numerical model of the Rio Negro-Solimões confluence we can see that the shear layer is moving upwards in downstream direction, see Figure 36. This is in agreement with what was seen previously in the numerical models for a very schematized confluence (Figure 14). According to the numerical model this interface should reach the surface just downstream of the boils. On the aerial photographs of this confluence this process is therefore hard to distinguish as it is masked by the upwelled water from the boils, see Figure 39. Figure 38 shows an aerial photograph during high flow, showing no boils and no signs of overturning, similar to the model.

Table 2 Overview of the Aerial Photographs used with an indication if boils were present on the photograph and/or upwelling of Solimões water was present at the Negro bank, all photographs are available through Google Earth, photographs were made by USGS, DigitalGlobe or CNES/Astrium.

Date	Boils present	Upwelling near bank present
1/1/1970	+[1]	-
25/7/2003	-	-
25/8/2004	+[1]	-
22/6/2005	-	-
3/7/2007	-	-
24/11/2007	+	-
26/10/2009	+[2]	-
2/8/2010	+[3]	-
2/10/2011[4]	-	-
31/7/2012	-	-
23/1/2013	+	+
7/8/2013	-	-
1/10/2013[4]	-	-
14/6/2014	-	-
14/8/2014[4]	-	-
30/11/2014	+	+
15/6/2015	-	-
2/7/2015	-	-

1. Only very close to the middle of the channel
2. Edge of photograph located just downstream of the boils
3. One Boil location, directly next to the mixing layer
4. Unclear Photograph

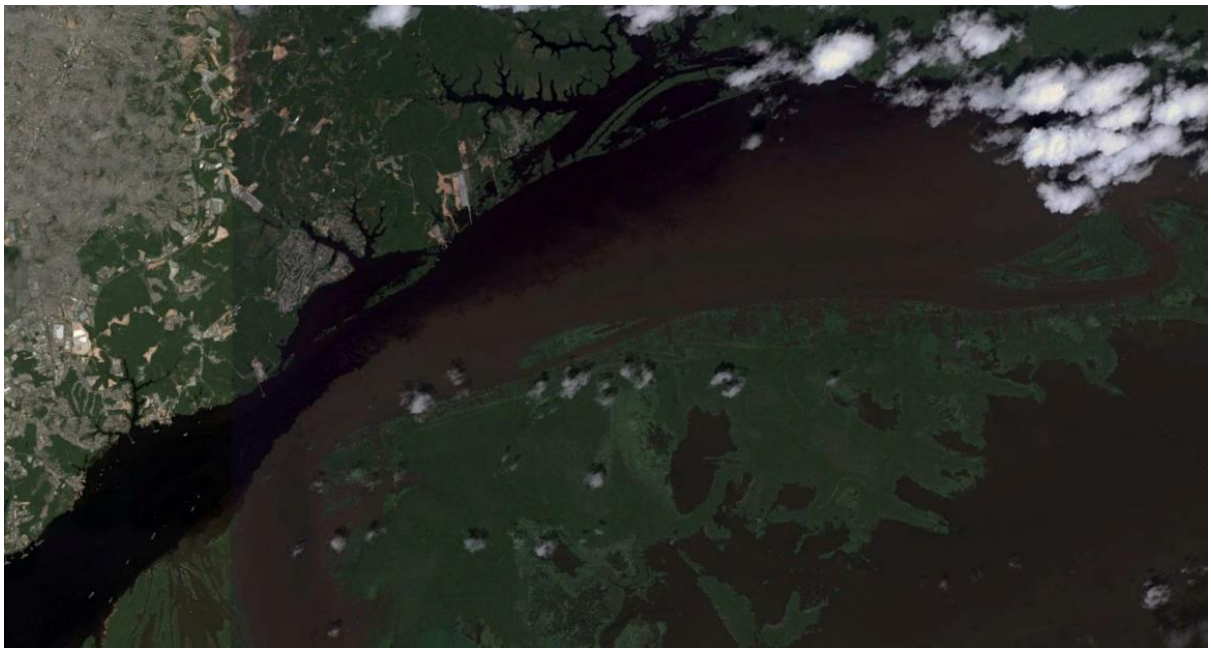

Figure 38 Aerial photograph of the Rio Negro – Solimões confluence on 15 June 2015 (high flow period), source: DigitalGlobe

The Rio Negro - Solimões confluence is famous for the lack of mixing at the surface between the two different coloured waters. This can for instance be seen in Figure 41 showing nearly no mixing at the surface of the confluence. It also shows floating foam around the shear layer indicating that downwelling is likely occurring here, a fact also seen from the instabilities just below the water

surface which are likely due to the shearing due to the vertical velocity differences. All of this shows large similarities with what we saw around the shear layer at the surface in the models, see Figure 28.

This theory is in disagreement with the theory of Trevethan et al. [2016] who claim that lateral stratification is caused by the water being pushed together. They made a conceptual model which states that the lateral forces of the two tributary discharges can cause lateral stratification at the shear layer.

Figure 39 Aerial photograph of the Rio Negro – Solimões confluence. Left part 3 July 2007 (high flow), Right part 24 November 2007 (highest momentum ratio). Source DigitalGlobe

In Figure 40 the points corresponding to the flow stages used are plotted into the diagram of Figure 30. Note that the velocity and depth are not uniform for each of the tributaries and as a result these points may be somewhat inaccurate. The locations of these points tell us that a mixing layer at the surface should not be visible in all of the runs used, in reality also other flow regimes occur during which a mixing layer may develop. This is in agreement with the models and the photographs.

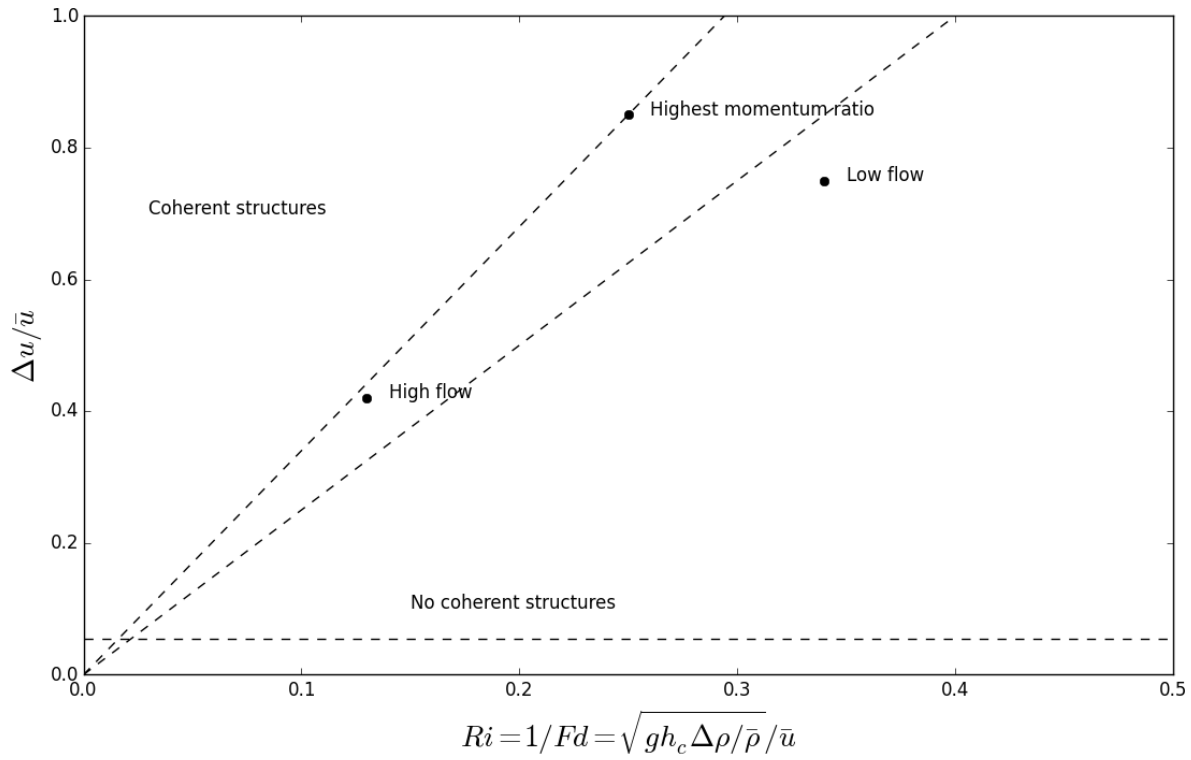

Figure 40 The points corresponding to the researched flow stages of the Rio Negro – Solimões confluence plotted in the diagram of Figure 30.

Figure 41 Photograph of the Meeting of the waters, the merging of the Solimões (right) and the Rio Negro (left), showing floating foam around the shear layer and flow instabilities below the water surface. Source: http://www.panoramio.com/photo/90000345

On the aerial photographs at some points in time (only during low water) upwelling of Solimões water occurred at the Rio Negro bank. This never occurred in the models. The models only used

representative values for the chosen months however. Even within a month the discharge could change significantly and between the same months of different years the differences in discharge can be even larger (see Figure 9).

Looking at the sediment concentration data from ANA [2016] at Manacapuru (some 100 km upstream of the confluence) a large spread in sediment concentrations is possible. Even a sediment concentration larger than 1.3 kg/m^3 was measured. What this data however tells us primarily is that even though the used values are representative for the chosen months, a significant spread is occurring. E.g. one month a significantly higher sediment concentration can occur than in the same month a year before.

The density difference is not only dependent on the sediment concentration but also on the temperature. Very little data on temperatures is available and little is known how much they can change between the years.

Since the models used representative values and not the values of the moment that the photographs were taken some differences can be expected. Considering the large spread and little data the observed differences are not very remarkable. The models still describe how the system responds to the different flow regimes and this is in line with what we see in the photographs.

5. Conclusions

This study has shown that small density differences between two tributaries of a confluence can have a major impact on the flow downstream of the confluence. Therefore density differences can be of importance in studies concerning sediment or pollutant routing or in environmental studies near a confluence.

The aim of this research was to see when and how density differences are important in confluences with respect to other occurring flow structures. It was seen that dense water flowed under lighter water.

Due to an acceleration of the lighter water the height of the underlying denser water increased in downstream direction. The interface between these two waters thus moved upwards.

The acceleration can be explained using the two-layer model. When overall the water does not accelerate or decelerate the water level gradient compensates for the bed friction. If the shear on the interface between these two waters is less than the bed friction, which is generally the case, the denser water will decelerate and the lighter water will accelerate.

At some point downstream the interface between the two waters reached the surface. This causes a typical shape at the water surface. First the lighter water will obtain a larger width (at the surface) and more downstream the denser water will become wider again (at the surface). This shape is well visible on aerial photographs if the two tributaries have different colours.

If the river downstream of the confluence is insufficiently wide, another process can occur. If the dense or light water reaches the opposite bank this water can well up or down near the bank. This was also visible on aerial photographs of confluences where a colour difference was present between the tributaries.

The motion of the water due to density differences is perpendicular to the main flow direction. This motion hampers the development of coherent structures in the mixing layer. The development of coherent structures can be predicted using two non-dimensional parameters, namely the Richardson number and the velocity difference divided by the mean velocity.

Several of the described processes (light water flowing over heavy water, dense water reaching the surface, reduced development of the mixing layer) occur at the Rio Negro – Solimões confluence. Oblique and aerial photographs of this confluence show several of these processes. Based on the aerial photographs it seems that this is however not the only confluence where these processes occur.

6. Recommendations

This research is one of the first studies trying to identify effects that density differences can have on the hydrodynamics of a confluence. Because of this still many things are unknown and further research would help understanding confluences better.

In this research the influence of several parameters has been investigated (like the depth, density difference, roughness and velocity) but not all parameters (most notably the confluence angle or the influence of the width ratio of the tributaries) were investigated.

This study used numerical models and photographs of confluences in nature. It would be very interesting to see if similar flow patterns can be found in a small-scale laboratory setting. Also a field study of one of the confluences in which we saw that the found process (of denser water moving upwards) occurs during a period at which the process is likely to occur, could give more insight. Possibly also other confluences where the found process is likely to occur could be used as a field case.

This study only looked at river confluences where the density difference was caused by a difference in temperature or sediment concentration. In estuary junctions a density difference can also be caused by a difference in salinity. At estuary junctions both density profiles and flow velocity profiles can change in smaller time frames (smaller than the tidal period). The effects of these changes are currently unknown. These kinds of junctions raise the additional question what would happen if one or both of the tributaries is/are vertically stratified.

This research showed that if in a river lighter water is located above denser water the interface between these two waters moves upwards in downstream direction. The reason for this could be explained using the two-layer model. Looking at the two-layer model it is likely that water level gradient, bed friction and shear between the two layers are the dominant factors in this process. This research did however not investigate how fast the interface can move upwards. This would be a good topic for further research. It is possible that this process also occurs downstream of for instance a cooling water discharge.

This study was carried out using the Delft3D software. This software seems to be well equipped to solve the processes caused by small density differences in confluences. Other numerical models would require at least, in addition to being 3D, a turbulence closure model based on the eddy viscosity concept if this phenomenon is to be investigated.

If Delft3D is used, the density gradient is influenced by the eddy diffusivity. A good approximation of the density gradient can be achieved by using the HLES module. For large confluences disturbances at the inflow boundary are required to achieve the formation of turbulent structures.

7. References

Albayrak, I., *An Experimental Study of Coherent Structures, Secondary Currents and Surface Boils and Their Interrelation in Open-Channel Flow*, EPFL, 2008

ANA, *Hidroweb*, available at: http://hidroweb.ana.gov.br/default.asp, last visited at June 2016

Ardura, A., V. Gomes, A.R. Linde, J.C. Moreira, J.L. Horreo, E. Garcia-Vazquez, *The Meeting of Waters, a possible shelter of evolutionary significant units for Amazonian fish*, Conserv Genet 14:1185–1192, 2013

Ashmore, P. & G. Parker, *Confluence Scour in Coarse Braided Streams*, Water Resources Research, Vol. 19, No. 2, Pages 392-402, 1983

Benda, L., N.L. Poff, D. Miller, T. Dunne, G. Reeves, G. Pess & M. Pollock, *The Network Dynamics Hypothesis: How Channel Networks Structure Riverine Habitats*, Bioscience, Vol. 54, N. 5, 413-427, 2004

Benjamin, T.B., *Gravity currents and related phenomena*, J. Fluid Mech., vol. 31, part 2, pp. 209-248, 1968

Best, J.L. & I. Reid, *Seperation Zone at Open-Channel Junctions*, journal of hydraulic engineering 110(11) 1588-1594, 1984

Best, J.L., *Flow Dynamics at River Channel Confluences: Implications for Sediment Transport and Bed Morphology*, The Society of Economic Paleontologists and Mineralogists, 1987

Best, J.L., *Kinematics, topology and significance of dune-related macroturbulence: some observations from the laboratory and field*, Spec. Publs int. Ass. Sediment, 2005

Best, J.L., *personal communication*, July 14, 2016

Biron, P.M., A.G. Roy, J.L. Best & C.J. Boyer, *Bed morphology and sedimentology at the confluence of unequal depth channels*, Geomorphology 8 115-129, 1993

Biron, P.M., J.L. Best & A.G. Roy, *Effects of Bed Discordance on Flow Dynamics at Open Channel Confluences*, journal of hydraulic engineering 122(12) 676-682, 1996

Biron, P.M., A.S. Ramamurthy & S. Han, *Three-Dimensional Numerical Modelling of Mixing at River Confluences*, journal of hydraulic engineering 130(3) 243-253, 2004

Blettler, M.C.M., M.L. Amsler, I.E. de Drago, L.A. Espinola, E. Eberle, A. Paira, J.L. Best, D.R. Parsons & E.E. Drago, *The impact of significant input of fine sediment on benthic fauna at tributary junctions: a case study of the Bermejo–Paraguay River confluence, Argentina*, Ecohydrology, 2014

Boyer, C., A.G. Roy & J.L. Best, *Dynamics of a river channel confluence with discordant beds: Flow turbulence, bed load sediment transport, and bed morphology*, Journal of Geophysical Research, Vol. 111, 2006

Bradbrook, K.F., S.N. Lane & K.S. Richards*, Numerical simulation of three-dimensional, time-averaged flow structure at river channel confluences*, Water Resources Research, vol. 36, no. 9, pages 2731-2746, 2000a

Bradbrook, K.F., S.N. Lane, K.S. Richards, P.M. Biron & A.G. Roy, *Large Eddy Simulation of periodic flow characteristics at river channel confluences*, Journal of Hydraulic Research. Vol. 38, 2000b

Brown, G.L. & A. Roshko, *On density effects and large structure in turbulent mixing layers*, Journal of Fluid Mechanics, vol. 64, part 4, pp. 775-816, 1974

Coleman, J.M., *Brahmaputra River: Channel Processes and Sedimentation*, Sedimentary Geology, 1969

Commandeur, A.S., *Turbidity Currents in Reservoirs*, Delft University of Technology, 2015

Constantinescu, G., S. Miyawaki, B. Rhoads, A. Sukhodolov & G. Kirkil, *Structure of turbulent flow at a river confluence with momentum and velocity ratios close to 1: Insight provided by an eddy‐resolving numerical simulation*, Water Resources Research, Vol. 47, W05507, 2011

Cook, C.B. & M.C. Richmond, *Monitoring and Simulating 3-D Density Currents at the Confluence of the Snake and Clearwater Rivers*, Critical Transitions in Water and Environmental Resources Management: pp. 1-9, 2004

Daoyi, C. & G.H. Jirka, *Linear stability analysis of turbulent mixing layers and jets in shallow water layers*, Journal Of Hydraulic Research, Vol. 36, No. 5, 1998

Deltares, *Delft3D-FLOW, Simulation of multi-dimensional hydrodynamic flows and transport phenomena, including sediments: User Manual*, Deltares, 2014

Filizola, N., N. Spinola, W. Arruda, F. Seyler, S. Calmant & J. Silva, *The Rio Negro and Rio Solimões confluence point – hydrometric observations during the 2006/2007 cycle*, River, Coastal and Estuarine Morphodynamics: RCEM, 2009

Gerritsen, H., E.D. de Goede, F.W. Platzek, J.A.Th.M. van Kester, M. Genseberger & R.E. Uittenbogaard, *Validation Document Delft3D-FLOW, A software system for 3D flow simulations*, Deltares, 2008

Grigoriadis, D.G.E., E. Balaras & A.A. Dimas, *Large-eddy simulations of unidirectional water flow over dunes*, Journal of Geophysical Research, Vol. 114, 2009

Herrero, H.S., C.M. García, F. Pedocchi, G. López, R.N. Szupiany & C.E. Pozzi-Piacenza, *Flow structure at a confluence: experimental data and the bluff body analogy*, Journal of Hydraulic Research Vol. 54, No. 3 pp. 263–274, 2016

Huang, J., L.J. Weber & Y.G. Lai, *Three-Dimensional Numerical Study of Flows in Open-Channel Junctions*, Journal of Hydraulic Engineering, 128(3): 268-280, 2002

Jackson, R.G., *Sedimentological and fluid-dynamic implications of the turbulent bursting phenomenon in geophysical flows*, Journal of fluid mechanics, vol. 77, part 3, pages 531-560, 1976

Kirkil, G., *Flow Structure in a Mixing Layer Developing over Flat Bed at High Reynolds Numbers*, E-proceedings of the 36th IAHR World Congress, 2015

Kneller, B.C., S.J. Bennett & W.D. McCaffrey, *Velocity structure, turbulence and fluid stresses in experimental gravity currents*, Journal of Geophysical Research, Vol. 104, No. C3, Pages 5381-5391, 1999

Kolmogorov, A. N., *Equations of turbulent motion in incompressible fluid.,* Izv. Akad. Nauk. SSR, Seria fizicheska Vi No.1 2 (1-2): 56–58., 1942, English translation: Imperial College, Mech. Eng. Dept. Rept. ON/6. 216, 326, 1968

Kranenburg, C., *Dichtheidsstromen*, TU Delft, 1998

Laraque, A., J.L. Guyot & N. Filizola, *Mixing processes in the Amazon River at the confluences of the Negro and Solimões Rivers, Encontro das Águas, Manaus, Brazil*, Hydrol. Process. 23, 3131–3140, 2009

Lefebvre, A., A.J. Paarlberg & C. Winter, *Flow separation and shear stress over angle-of-repose bed forms: A numerical investigation*, Water Resour. Res., 50, 986–1005, 2014

Lyubimova, T., A. Lepikhin, V. Konovalov, Ya. Parshakova & A. Tiunov, *Formation of the density currents in the zone of confluence of two rivers*, Journal of Hydrology 508 328–342, 2014

McLelland, S.J., P.J. Ashworth & J.L. Best, *The origin and downstream development of coherent flow structures at channel junctions*, In book: Coherent Flow Structures in Open Channels, Chapter: 23, Publisher: John Wiley and Sons Ltd, 1996

Miyawaki, S., G. Constantinescu, B. Rhoads & A. Sukhodolov, *Changes in Three-Dimensional Flow Structure at a River Confluence with Changes in Momentum Ratio*, River Flow, 2010

Molinier, M., J.L. Guyot, V. Guimarães & E. de Oliveira, *Hydrologie du bassin de l'Amazone*, Colloque Grands Bassins Fluviaux. PEGI. Paris. 22-24, 1993

Molinier, M., J.L. Guyot, E. de Oliveira & V. Guimarães, *Les régimes hydrologiques de l'Amazone et de ses affluents*, L'hydrologie tropicale: géoscience et outil pour le développement, 1996

Nezu, I. & H. Nakagawa, *Turbulence in Open-Channel Flows*, A.A. Balkema Rotterdam, 1993

Nezu, I., A. Tominaga & H. Nakagawa, *Field Measurements of Secondary Currents in Straight Rivers*, J. Hydraul. Eng., 119(5): 598-614, 1993

Omidyeganeh, M. & U. Piomelli, *Coherent structures in the flow over two-dimensional dunes*, Direct and Large-Eddy Simulation VIII, 2011

Prandtl, L., *Über ein neues Formelsystem für die ausgebildete Turbulenz,* Nachrichten von der Akademie der Wissenschaften in Gottingen. Mathematisch-Physikalische Klasse pages 6–19. 216, 326, 1945

Prooijen, van, B.C. & W.S.J. Uijttewaal, *A linear approach for the evolution of coherent structures in shallow mixing layers*, Physics Of Fluids, Vol. 14, No. 12, 2002

Richey, E.J., R.H. Meade, E. Salati, A.H. Devol, C.F. Nordin Jr. & U. Dos Santos, *Water discharge and suspended sediment concentrations in the Amazon river: 1982-1984*, Water resources research, Vol. 22, No. 5, Pages 756-764, 1986

Rhoads, B.L. & S.T. Kenworthy, *Flow structure at an asymmetrical stream confluence*, Geomorphology 11 273-293, 1995

Rhoads, B.L. & A.N. Sukhodolov, *Field investigation of three-dimensional flow structure at stream confluences: 1. Thermal mixing and time-averaged velocities*, Water Resources Research, Vol. 37, No. 9, Pages 2393–2410, 2001

Rhoads, B.L. & A.N. Sukhodolov, *Spatial and temporal structure of shear layer turbulence at a stream confluence*, Water Resources Research, vol. 40, 2004

Rhoads, B.L. & A.N. Sukhodolov, *Lateral momentum flux and the spatial evolution of flow within a confluence mixing interface*, Water Resources Research, vol. 44, 2008

Schijf, J.B. & J.C. Schönfeld, *Theoretical considerations on the motion of salt and fresh water*, Minnesota International Hydraulics Convention, 1953

Serres, De, B., A.G. Roy, P.M. Biron & J.L. Best, *Three-dimensional structure of flow at a confluence of river channels with discordant beds*, Geomorphology 26 313–335, 1998

Shin, J.O., S.B. Dalziel & P.F. Linden, *Gravity currents produced by lock exchange*, J. Fluid Mech. , vol. 521, pp. 1–34., 2004

Sukhodolov, A.N. & B.L. Rhoads, *Field investigation of three-dimensional flow structure at stream confluences 2. Turbulence*, Water Resources Research, Vol. 37, No. 9, Pages 2411-2424, 2001

Trevethan, M., M. Ianniruberto, M. Oliveira, A. Martinelli, N. Filizola, C. Gualtieri, *Hydrodynamic and morphodynamic features observed about the confluence of the Negro and Solimões Rivers, Brazil*, 9th Symposium on River, Coastal and Estuarine Morphodynamics (RCEM 2015), At Iquitos, Peru, 2015a

Trevethan, M., A. Martinelli, M. Oliveira, M. Ianniruberto & C. Gualtieri, *Fluid Mechanics, Sediment Transport And Mixing About The Confluence Of Negro And Solimões Rivers, Manaus, Brazil*, E-proceedings of the 36th IAHR World Congress, The Hague, 2015b

Trevethan, M., R.V. Santos, M. Ianniruberto, M. Oliveira, A. Martinelli & C. Gualteri, *Influence Of Tributary Water Chemistry On Hydrodynamics And Fish Biogeography About The Confluence Of Negro And Solimoes Rivers, Brazil*, 11th ISE 2016, Melbourne, Australia, 2016

Uijttewaal, W.S.J., R. Booij, *Effects of shallowness on the development of free-surface mixing layers*, Physics of Fluids, Vol. 12, N. 2, 2000

Vermaas, D.A., W.S.J. Uijttewaal & A.J.F. Hoitink, *Lateral transfer of streamwise momentum caused by a roughness transition across a shallow channel*, Water Resources Research, Vol. 47, 2011

Vreugdenhil, C.B., Computation of gravity currents in estuaries, TU Delft, 1970

Winant, C.D. & F.K. Browand, *Vortex pairing: the mechanism of turbulent mixing layer growth at moderate Reynolds number*, Journal of Fluid Mechanics, vol. 63, part 2, pages 237-255, 1974

Zedler, E.A. & R.L. Street, *Large-Eddy Simulation of Sediment Transport: Currents over Ripples*, Journal of Hydraulic Engineering, 127(6): 444-452, 2001

A. Overview of model runs used

A.1 Validation of software

Validation of HLES
Chézy roughness: 60 $m^{0.5}/s$
Depth: 35 m
Mean velocity: 1.19 m/s
Temperature: 30°C
Temperature difference: 0 °C
Turbulence model: k-ε
Velocity ratio: 3/7
HLES: enabled, relaxation time 40 min.
Non-hydrostatic: disabled

Requirement for non-hydrostatic
Chézy roughness: 60 $m^{0.5}/s$
Depth: 35 m
Mean velocity: 1.19 m/s
Temperature: 30°C
Temperature difference: 2 °C
Turbulence model: k-ε
Velocity ratio: 1
HLES: disabled
Non-hydrostatic: disabled (σ-layers & z-layers) & enabled

A.2 General schematized model

Baseline model run:
Chézy roughness: 60 $m^{0.5}/s$
Depth: 35 m
Mean velocity: 1.19 m/s
Velocity ratio: 1
Temperature: 30°C
Temperature difference: 2 °C
Turbulence model: k-ε
HLES: enabled, relaxation time 40 min.

Velocity ratio changed runs:
Baseline but velocity ratio changed to 3/7, 7/13, 2/3, 9/11,11/9, 3/2, 13/7 and 7/3.

Temperature difference changed runs:
Baseline but temperature difference changed to 0.5 – 4 °C with steps of 0.5 °C.

Roughness changed runs:
Baseline but Chézy roughness changed to 40 – 80 $m^{0.5}/s$ with steps of 10 $m^{0.5}/s$.

Depth changed runs:
Baseline but depth changed to 20 – 65 m with steps of 5 m.

Velocity changed runs:
Baseline but velocity changed to 0.676 – 1.859 m/s with steps of 0.169 m/s.

Width changed runs:
Baseline but width changed to 1230 m.

Turbulence model runs:
Baseline but instead of k-ε model the constant eddy viscosity model, k-L model or Algebraic model were used.

Velocity ratio with density difference runs:
Baseline with varying velocity ratio and temperature difference

		Temperature difference (°C)				
		0.5	1	2	2.5	3
Velocity ratio	7/3	✔	✔	✔	✔	✔
	13/7	✔	✔	✔	✔	
	3/2	✔	✔	✔		

Velocity ratio with depth runs:
Baseline with varying velocity ratio and depth. Note that the three models in the column of depth 35 m are the same as those in the table above with a temperature difference of 2 °C.

		Depth (m)			
		17.5	25	35	52.5
Velocity ratio	7/3	✔	✔	✔	✔
	13/7	✔		✔	
	3/2	✔		✔	

B. Analysis of LANDSAT imagery

Based on LANDSAT, available at: http://landsatlook.usgs.gov/viewer.html

Date Photo	Boils	Upwelling near bank
18/2/2016	+/-	+/-
30/11/2015	+/-	-
23/11/2015	-	-
22/10/2015	+	+/-
27/9/2015	+/-	-
11/9/2015	-	-
10/8/2015	-	-
18/7/2015	-	-
9/7/2015	-	-
2/7/2015	-	-
16/6/2015	-	-
7/6/2015	-	-
22/5/2015	-	-
20/4/2015	-	-
15/2/2015	+/-	+/-
30/1/2015	+/-	+
7/1/2015	+	+
22/12/2014	+	+/-
13/12/2014	+	-
11/11/2014	-	-
8/9/2014	-	-
1/9/2014	-	-
23/8/2014	-	-
31/7/2014	-	-
22/7/2014	-	-
6/7/2014	-	-
12/6/2014	-	-
28/5/2014	-	-
9/3/2014	+/-	-
28/2/2014	+	+
27/1/2014	+	+
4/1/2014	+	+/-
10/12/2013	+/-	-
3/12/2013	+/-	-
24/11/2013	+/-	-
16/10/2013	-	-
7/10/2013	-	-
14/9/2013	-	-
5/9/2013	-	-
4/8/2013	-	-
19/7/2013	-	-
12/7/2013	-	-
17/6/2013	-	-
16/5/2013	-	-
14/4/2013	-	-
16/9/2011	-	-
31/8/2011	-	-

14/7/2011	-	-
25/4/2011	+/-	-
24/3/2011	-	-
8/3/2011	+	-
8/10/2010	-	-
28/8/2010	-	-
27/7/2010	-	-
9/6/2010	-	-
29/11/2009	+/-	-
5/10/2009	+/-	-
26/9/2009	-	-
10/9/2009	-	-
25/8/2009	-	-
2/8/2009	-	-
24/7/2009	-	-
1/7/2009	-	-
5/5/2009	-	-
3/4/2009	-	-
12/12/2008	-	-
10/11/2008	-	-
7/9/2008	-	-
22/8/2008	-	-
6/8/2008	-	-
21/7/2008	-	-
11/1/2008	+/-	-
21/9/2007	-	-
4/8/2007	-	-
17/6/2007	-	-
7/5/2007	+/-	-
16/12/2006	+	+/-
29/10/2006	-	-
27/9/2006	-	-
11/9/2006	-	-
2/9/2006	-	-
16/7/2006	-	-
30/6/2006	-	-
29/5/2006	-	-
17/10/2005	-	-
10/10/2005	-	-
24/9/2005	-	-
8/9/2005	-	-
23/8/2005	-	-
29/7/2005	-	-
27/6/2005	-	-
20/6/2005	-	-
11/6/2005	-	-
8/4/2005	-	-
19/2/2005	+	+
11/1/2005	+	+
10/12/2004	+/-	-
24/11/2004	+	-

30/10/2004	-	-
23/10/2004	-	-
14/10/2004	-	-
28/9/2004	-	-
26/7/2004	-	-
10/7/2004	-	-
24/6/2004	-	-
26/2/2004	+	-
1/2/2004	+	+
31/12/2003	+	+/-
24/12/2003	+	-
13/11/2003	-	-
21/10/2003	+/-	-
19/9/2003	-	-
10/9/2003	-	-
25/8/2003	-	-
9/8/2003	-	-
24/7/2003	-	-
8/7/2003	-	-
22/5/2003	-	-
13/5/2003	-	-
26/3/2003	+/-	-
22/2/2003	+/-	+
15/2/2003	+	+
21/1/2003	+	+
5/1/2003	+	+/-
27/11/2002	+/-	-
11/11/2002	-	-
26/10/2002	-	-
10/10/2002	-	-
24/9/2002	-	-
15/9/2002	-	-
8/9/2002	-	-
30/8/2002	-	-
14/8/2002	-	-
7/8/2002	-	-
29/7/2002	-	-
22/7/2002	-	-
6/7/2002	-	-
20/6/2002	-	-
11/6/2002	-	-
19/5/2002	-	-
17/4/2002	-	-
8/4/2002	+/-	+/-
16/3/2002	+/-	+
8/3/2002	+/-	+
28/2/2002	+	+
18/1/2002	+	+
10/12/2001	+	+
1/12/2001	+/-	+/-
24/11/2001	-	-

15/11/2001	-	-
7/11/2001	+/-	-
23/10/2001	-	-
15/10/2001	-	-
14/10/2001	-	-
7/10/2001	-	-
12/9/2001	-	-
5/9/2001	-	-
28/8/2001	-	-
20/8/2001	-	-
11/8/2001	-	-
4/8/2001	-	-
27/7/2001	-	-
26/7/2001	-	-
19/7/2001	-	-
11/7/2001	-	-
3/7/2001	-	-
17/6/2001	-	-
21/3/2001	+	+
13/3/2001	+	+
23/12/2000	+	+
7/12/2000	+/-	-
29/11/2000	-	-
13/11/2000	-	-
12/11/2000	-	-
4/11/2000	-	-
27/10/2000	-	-
19/10/2000	-	-
12/10/2000	-	-
4/10/2000	-	-
10/9/2000	-	-
25/8/2000	-	-
17/8/2000	-	-
9/8/2000	-	-
8/7/2000	-	-
30/6/2000	-	-
4/5/2000	+/-	-
9/3/2000	+	+
29/12/1999	+	+
12/12/1999	+	+
5/12/1999	+	-
26/11/1999	-	-
2/11/1999	-	-
26/10/1999	-	-
17/10/1999	-	-
10/10/1999	-	-
2/10/1999	-	-
24/9/1999	-	-
16/9/1999	-	-
8/9/1999	-	-
30/8/1999	-	-

23/8/1999	-	-
6/8/1999	-	-
30/7/1999	-	-
21/7/1999	-	-
13/7/1999	-	-
27/6/1999	-	-
17/4/1999	-	-
28/9/1998	-	-
26/7/1998	-	-
16/2/1998	+/-	+
27/10/1997	+/-	+/-
23/7/1997	-	-
7/7/1997	-	-
21/6/1997	-	-
9/11/1996	+/-	+
6/9/1996	-	-
21/8/1996	-	-
5/8/1996	-	-
20/7/1996	-	-
27/6/1996	-	-
26/5/1996	-	-
15/10/1995	-	-
20/9/1995	+/-	-
28/8/1995	-	-
19/10/1994	+/-	-
2/3/1994	+	+
6/10/1992	-	-
2/7/1992	+/-	-
29/5/1991	-	-
20/12/1990	+	+
22/9/1990	-	-
30/8/1990	-	-
20/7/1990	+	-
30/3/1990	+	+
1/12/1989	+	-
21/10/1989	-	-
2/8/1989	-	-
1/7/1989	-	-
30/7/1988	-	-
20/1/1988	+	+
14/9/1987	-	-
15/5/1986	+/-	-
24/11/1984	-	-
30/7/1984	-	-

C. Formula for the calculation of water density

In this appendix a formula for the calculation of the density of water due to temperature and sediment concentration will be derived.
Kranenburg [1998] states that the density of water can be approximated, under the assumption that the water density is only affected by the temperature and the salinity, by the formula:

$$\rho \approx 1000 + 0.805\sigma - 0.0166(T - 4 - 0.212\varsigma)^{1.69}$$

Setting the salinity to 0 we get an expression for the density of water due to temperature changes:

$$\rho \approx 1000 - 0.0166(T - 4)^{1.69}$$

Sediment particles in the water increase the weight by the weight of the sediments. The density thus increases by the sediment concentration. However the volume that the sediments now occupy is no longer occupied by water. The fraction of the total volume that the sediment particles occupy is:

$$V_S = \frac{\sigma}{\rho_s}$$

The volume of water in 1 m^3 is thus 1-V_s
The final formula now becomes:

$$\rho \approx \sigma + (1 - \frac{\sigma}{\rho_s})(1000 - 0.0166(T - 4)^{1.69})$$

D. Boils in stratified water column

D.1 Introduction

In the Amazon about 7 km downstream of the confluence of the Rio – Negro and Solimões rivers boils of Solimões water erupting within the Rio Negro water could be seen. It is known that due to temperature and sediment concentration differences the Solimões water is heavier than the Rio Negro water (paragraph 7.3). Due to this density difference the Solimões water flows underneath the Rio Negro water (paragraph 8.1). At the location where the boils are initiated the water is thus vertically stratified. It is expected that the boils are caused by the flapping of the shear layer behind permanent bed level disturbances similar to boils occurring downstream of bed forms (as described by Best et al. [2005]).

The mechanism behind boils behind a bed disturbance has already been investigated in quite some detail [Coleman, 1969; Jackson, 1976; Nezu & Nakagawa, 1993; Best et al., 2005; Grigoriadis et al., 2009; Omidyeganeh & Piomelli, 2011]. These researches were based on models or field investigations. None of these studies however investigated if boils can be present when the water is vertically stratified. As boils can increase mixing, they can in some cases be of importance. One of these cases could be the confluence of the Rio Negro – Solimões or in estuary systems.

The aim of this appendix is to give an indication how an investigation into the occurrence of boils in a stratified water column can be undertaken. For some arguments it is assumed Delft3D will be used, even though this may not be the most suitable software available (right now).

D.2 How to set-up the research

Different models can be used to identify what the occurrence is with and without stratification. Optionally the rate of stratification (parameterized with the Richardson number) can also be changed systematically to identify how the occurrence depends on the level of stratification.

Boils occur due to the change of location of the reattachment point of the eddy formed behind the bed form. This reattachment point shifts in location due to the fact that between the eddy and the normal flow a mixing layer will develop. This mixing layer will thus need to be resolved, and a large eddy simulation (LES) is thus required. All previous numerical investigations into the formation of boils used LES as well [Zedler & Street, 2001; Grigoriadis et al., 2009; Omidyeganeh & Piomelli, 2011]. The eddy behind a bed form can be resolved by Delft3D in a RANS calculation [Lefebvre et al., 2014].

No LES in Delft3D attempt is known by the author. A LES in Delft3D should however be possible: *"The equations of Delft3D-FLOW are capable of resolving the turbulent scales (large eddy simulation), but usually the hydrodynamic grids are too coarse to resolve the fluctuations. Therefore, the basic equations are Reynolds-averaged introducing so-called Reynolds stresses. These stresses are related to the Reynolds-averaged flow quantities by a turbulence closure model"* [Deltares, 2014]. If Delft3D will be used it is advisable to first check if it is able to run LES satisfactorily.

The mixing layer forming behind the bed form is influenced greatly by turbulent structures already present in the flow upstream. For the model this means that at the inflow boundaries turbulent structures should be present. Turbulent structures tend to have a certain length and time scale. At the inflow boundaries the discharge cannot be purely stochastic, but it should be both time and space correlated.

Note that the present version of Delft3D has an inefficient way of handling boundary files for such cases. It loads the entire boundary file upon the start of a run into the RAM. This is very efficient for the computational time. However if for each time step for each grid cell (both in the horizontal and vertical) a value needs to be read the RAM fills up rapidly. Actually the RAM might limit the size of the open boundary and/or the simulation time. If only the parts of the boundary file are read at the time they are needed in the simulation (and after they are used deleted from RAM) the simulation time and/or size of the open boundary is no longer limited by the amount of RAM installed. Note that this solution will slightly increase computational time.

Z-layers do not follow the bed level geometry as well as σ-layers. However significant vertical accelerations could occur. If these accelerations occur the non-hydrostatic solver should be enabled which is only possible using z-layers. A first step would thus be to test if the non-hydrostatic solver is required and based on that decide on the vertical discretization. Regardless of the choice for vertical discretization, thinner layers closer to the bottom and the region where the density gradient is largest, is recommended as these areas are of most importance. The maximum number of layers in Delft3D is 100, which thus limits the vertical grid size.